Electroproduction of inclusive pions at high Q^2 *

C. J. Bebek, C. N. Brown,[†] R. V. Kline, F. M. Pipkin, S. W. Raither, and L. K. Sisterson[‡]

High Energy Physics Laboratory, Harvard University, Cambridge, Massachusetts 02138

A. Browman,[§] K. M. Hanson,[§] D. Larson, and A. Silverman

Laboratory of Nuclear Studies, Cornell University, Ithaca, New York 14853

(Received 6 June 1977; revised manuscript received 8 August 1977)

This paper reports measurements of the inclusive pion electroproduction reaction $e + N \to e + \pi^{\pm} +$ anything with both proton and neutron targets for pions produced along and near the direction of the virtual photon. Two independent purposes of these measurements were to provide data at low ϵ and at high Q^2. Data are reported for the (W, Q^2, ϵ) points (2.2 GeV, 1.2 GeV², 0.45), (2.7, 2.0, 0.35), (2.7, 3.3, 0.40), (2.7, 6.2, 0.40), and (2.7, 9.5, 0.40). The data are used to test Feynman scaling and to compare the ratio of the cross sections for charged-pion production to the quark-model predictions. The data are also used in conjunction with the data from earlier experiments to separate the scalar and transverse components of the cross section.

I. INTRODUCTION

The elastic scattering of electrons was first used by Hofstadter to measure the charge distribution of the proton.[1] These measurements suggested a homogeneous object and gave no evidence of a pointlike core. The early inelastic electron scattering measurements carried out at Stanford, CEA, and DESY showed a rich spectrum of excited states starting with the $\Delta(1236)$. Higher energy elastic scattering measurements carried out at the Stanford Linear Accelerator Center confirmed the absence of a proton core.[2] The inelastic scattering measurements of the reaction

$$e^- + p \to e^- + \text{anything} \tag{1}$$

showed, however, that the proton was not a simple object and that it acted as if it contained pointlike structures.[3-6]

If it is assumed that electron-proton scattering is correctly described by the one-photon approximation in which the interaction is mediated by a single virtual photon, the differential cross section for reaction (1) in the laboratory frame can be written in the form

$$\frac{d^2\sigma}{d\Omega dE'} = \frac{4\alpha^2(E')^2}{Q^4} [W_2(Q^2, \nu)\cos^2(\tfrac{1}{2}\theta)$$
$$+ 2W_1(Q^2, \nu)\sin^2(\tfrac{1}{2}\theta)], \tag{2}$$
$$= \Gamma [\sigma_t(Q^2, \nu) + \epsilon \sigma_s(Q^2, \nu)], \tag{3}$$

where

$$Q^2 = 4EE' \sin^2(\tfrac{1}{2}\theta), \tag{4}$$
$$\nu = E - E', \tag{5}$$
$$\epsilon = [1 + 2(1 + \nu^2/Q^2)\tan^2(\tfrac{1}{2}\theta)]^{-1}, \tag{6}$$

and

$$\Gamma = \frac{\alpha}{4\pi^2} \frac{E'}{E} \frac{W^2 - M^2}{MQ^2} \left(\frac{1}{1 - \epsilon} \right). \tag{7}$$

Here Q^2 and ν are the negative mass squared and the energy of the virtual photon, respectively, ϵ is a measure of the photon polarization, W_1 and W_2 are the proton structure functions, and σ_t and σ_s are, respectively, the contributions to the equivalent total virtual-photoproduction cross section for transverse and scalar photons.

The SLAC experiments showed three surprising results. First, at high Q^2, νW_2 was much larger than the nucleon form factors found from elastic electron-proton scattering. Second, $\nu W_2(Q^2, \nu)$ and $W_1(Q^2, \nu)$ were a function of the single variable $\omega = 2M\nu/Q^2$ and, for $\omega > 4$, $\nu W_2(\omega)$ was found to be nearly independent of ω. Third, the scalar cross section σ_s was found to be much smaller than σ_t. The first result led to the description of the proton as an assembly of pointlike constituents which are called partons.[7,8] The second result, scaling, which confirmed an earlier dimensional analysis by Bjorken,[9] supports the parton-model picture. The third result indicates that the partons are predominantely spin-$\tfrac{1}{2}$ particles. The specific model in which the partons are quarks has been quite successful in explaining the single-arm data.

The experiment reported in this paper is the third of a series of experiments carried out at the Wilson Synchrotron Laboratory at Cornell University in which a single pion, kaon, or proton is detected in coincidence with the scattered electron. One of the purposes of these experiments is to determine how reactions with specific hadrons in the final state contribute to the scaling of νW_2. Other motivations are to test the extension of the parton-quark model to single-hadron inclusive reactions by measuring the π^+/π^- ratio, the relative cross sections from neutron and proton tar-

gets, and the ratio of the scalar to transverse cross sections. The data can also be used to test for Feynman scaling and limiting fragmentation. This paper represents a more extensive report on data reported earlier[10-12] and relates in succession the underlying kinematics, the simple parton-model theory, the apparatus, the analysis of the data, the results of the measurements, and a summary of the conclusions.

II. KINEMATICS

This paper reports the results for the inclusive reactions

$$e^- + N \to e^- + \pi^{\pm} + X, \tag{8}$$

where N, the target nucleon, can be a proton, neutron, or deuteron and X denotes all the undetected particles. The deuteron is referred to as a nucleon in the sense that it is a simple composite of a proton and a neutron. We now write the general form of the cross section for reaction (8), assuming that only the one-photon-exchange diagram of Fig. 1 contributes to the cross section. Experiments which show that the radiatively corrected inelastic scattering cross sections for electrons and positrons are equal for Q^2 as large as 15 GeV^2 give evidence for the validity of the one-photon-exchange hypothesis.[13] With the variables defined in Figs. 1 and 2 and Table I, the differential cross section for reaction (8) is

$$\frac{d^5\sigma}{dE'd\Omega'dp_h{}^3} = \frac{E'}{16EM(2\pi)^3}|\mathfrak{M}|^2$$
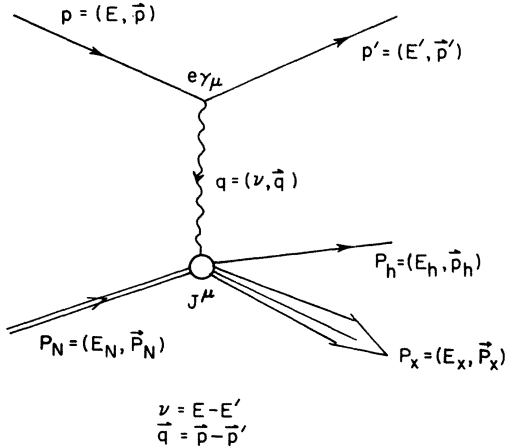
$$\times \delta((q + P_N - P_h)^2 - M_X{}^2), \tag{9}$$

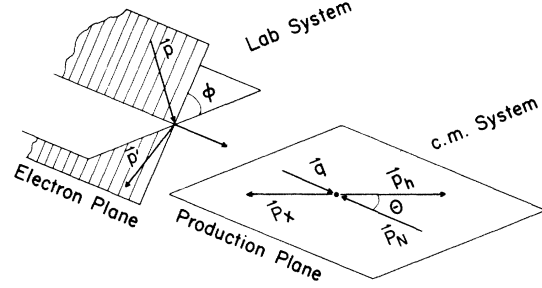FIG. 1. Schematic diagram for the electroproduction reaction $e + p \to e + h + X$.

FIG. 2. Schematic diagram showing electron scattering plane and hadron production plane for the reaction $e + p \to e + h + X$ and the notation used to describe this reaction.

where the matrix element, $\mathfrak{M}$, is written

$$\mathfrak{M} = \bar{u}(p')\gamma_\mu u(p)\frac{e^2}{Q^2}\langle P_h, P_x|J^\mu|P_N\rangle. \tag{10}$$

The u's are the electron spinors and J^μ is the hadron current. Averaging over initial and summing over final spin states we obtain for the square of the matrix element the expression

$$|\mathfrak{M}|^2 = \frac{2e^4}{Q^4}\left(p_\mu p'_\nu + p_\mu p'_\nu - q_{\mu\nu}\frac{Q^2}{2}\right)T^{\mu\nu}$$

$$= \frac{2e^4}{Q^4}L_{\mu\nu}T^{\mu\nu}, \tag{11}$$

where $L_{\mu\nu}$ describes the electron vertex and $T^{\mu\nu}$ describes the hadron vertex depicted in Fig. 1. The important feature of Eq. (11) is that the two vertices factor; this allows us to treat reaction (8) as the virtual photoproduction reaction[14-16]

$$\gamma_v + N \to \pi^{\pm} + X. \tag{12}$$

Returning to Eq. (10) and projecting out the three photon polarizations, the cross section (9) can be written

TABLE I. Definition of kinematic variables for $e + p \to e + p +$ anything.

E	Incident electron energy
E'	Scattered electron energy
θ_e	Electron scattering angle
ν	Virtual-photon laboratory energy
Q^2	Virtual-photon negative mass squared
ϵ	Virtual-photon polarization parameter
W	Virtual-photon–target-nucleon system invariant mass
E_h	Detected hadron energy
P_h	Detected hadron momentum
θ	Virtual-photon–hadron polar angle
ϕ	Virtual-photon–hadron azimuth angle
$M_X{}^2$	Invariant undetected mass squared

$$\frac{d^5\sigma}{dE'd\Omega'dp_h^3} = \Gamma \frac{d^3\sigma}{dp_h^3} , \tag{13a}$$

$$\frac{d^3\sigma}{dp_h^3} = \left[\frac{d\sigma_t}{dp_h^3} + \epsilon\frac{d\sigma_s}{dp_h^3} + \epsilon\frac{d\sigma_{tt}}{dp_h^3} \cos(2\phi)\right.$$

$$\left. + \left(\frac{\epsilon + \epsilon^2}{2}\right)^{1/2}\frac{d\sigma_{ts}}{dp_h^3} \cos\phi\right] , \tag{13b}$$

where Γ is the flux of transverse photons and ϵ is the linear transverse polarization of the photons. The longitudinal polarization is given by

$$\epsilon_L = (Q^2/\nu^2)\epsilon . \tag{14}$$

The four cross sections in Eq. (13) are the contributions from transverse photons, longitudinal photons, the interference of the two transverse amplitudes, and the interference of the longitudinal and transverse amplitudes.

III. THEORY

A. Structure function

The invariant structure function is defined as

$$F(p_L^*, p_T, W) = \frac{E_h}{\sigma_{tot}}\frac{d^3\sigma}{dp_h^3} = \frac{E_h^*}{\sigma_{tot}}\frac{2}{p_{max}^*}\frac{d^3\sigma}{dx\,dp_T^2 d\phi}$$

$$= \frac{E_h^*}{\sigma_{tot}}\frac{2}{[(p_{max}^*)^2 - p_T^2]^{1/2}}\frac{d^3\sigma}{dx'dp_T^2 d\phi} , \tag{15}$$

where σ_{tot} is the total virtual photoproduction cross section. The Feynman scaling variable, x, is defined as the ratio of the hadron's momentum in the direction of the virtual photon to the kinematically maximum possible momentum calculated in the target-nucleon–virtual-photon rest frame by the equation

$$x = p_L^*/p_{max}^* . \tag{16}$$

Variables in the target-nucleon–virtual-photon rest frame are denoted by an asterisk. The variable, x', which is defined by the equation

$$x' = \frac{p_L^*}{[(p_{max}^*)^2 - p_T^2]^{1/2}} , \tag{17}$$

was invented so that a given missing mass would occur at a fixed value of x' for fixed W independent of the transverse momentum p_T. For the results presented here, p_T is small and $x' \simeq x$.

A note concerning the definition of x' is required before proceeding. There is an ambiguity in the definition of p_{max}^* for the π^- data. Conventionally, p_{max}^* has been defined by the $\pi^+ n$ channel for both π^+ and π^- even though p_{max}^* for π^- is kinematically determined by the $\pi^-\Delta$ channel. This is not important for large values of W but has the effect of compressing the x' range for π^- relative to that for

π^+ at the W values of this experiment. For the results presented here and in the earlier reports, we have deferred to convention and used the π^+-determined p_{max}^* for all the data.

1. x' dependence

Feynman hypothesized[17] that, in the limit of large W, F would become a function of x and p_T only,

$$F(p_L^*, p_T, W) \xrightarrow[W\to\infty]{} F(x, p_T) , \tag{18}$$

or, equivalently, a function of x' and p_T. In two earlier Harvard experiments,[18,19] Feynman scaling was found to be approximately true for pions in the forward direction ($p_T^2 \le 0.02$ GeV^2) for $1.2 \le Q^2 \le 4.0$ GeV^2 and $2.1 \le W \le 3.1$ GeV. This experiment extends the Q^2 test of scaling to 10 GeV^2.

In the Feynman quark model[8] the structure functions of the nucleons and the produced hadrons can be expressed in terms of the parton distribution and parton fragmentation functions. Let $u, d, s, \bar{u}, \bar{d}, \bar{s}$ denote the three quarks and their antiquarks and let $x_B = 1/\omega$. Define $u(x_B)dx_B$ as the number of u quarks with momentum between x_B and $x_B + dx_B$ with similar definitions for the other quarks. Further, define $D_i^h(x)$ as the number of hadrons of type h that fragment from quark type i with momentum between x and $x + dx$. The nucleon structure function for electron-proton scattering can then be written in terms of the distribution functions alone

$$f_{ep}(x_B) = \frac{4}{9}[u(x_B) + \bar{u}(x_B)] + \frac{1}{9}[d(x_B) + \bar{d}(x_B)]$$

$$+ \frac{1}{9}[s(x_B) + \bar{s}(x_B)] , \tag{19}$$

and for electron-neutron scattering

$$f_{en}(x_B) = \frac{1}{9}[u(x_B) + \bar{u}(x_B)] + \frac{4}{9}[d(x_B) + \bar{d}(x_B)]$$

$$+ \frac{1}{9}[s(x_B) + \bar{s}(x_B)] , \tag{20}$$

where the constants are the squares of the quark charges. The f's are related to the total inelastic cross section by

$$\nu W_2(x_B) = x_B f(x_B) , \tag{21a}$$

$$2MW_1(x_B) = f(x_B) . \tag{21b}$$

In the quark model the nucleons are composed of three valence quarks and a sea of quark-antiquark pairs. McElhaney and Tuan[20] have assumed that the quarks are distributed such that

$$u(x_B) = u_v(x_B) + c(x_B) , \tag{22a}$$

$$d(x_B) = d_v(x_B) + c(x_B) , \tag{22b}$$

$$s(x_B) = \bar{u}(x_B) = \bar{d}(x_B) = \bar{s}(x_B) = c(x_B) , \tag{22c}$$

where v denotes valence quarks and $c(x_B)$ is the distribution of quarks in the sea. Using phase-space

and Regge considerations they have fitted the total-cross-section data and found

$$u_v(x_B) = 1.74 x_B^{-1/2}(1 - x_B)^3(1 + 2.3 x_B) ,$$ (23a)

$$d_v(x_B) = 1.11 x_B^{-1/2}(1 - x_B)^{3 \cdot 1} ,$$ (23b)

$$c(x_B) = 0.10 x_B^{-1}(1 - x_B)^{7/2} .$$ (23c)

If we assume the factorization of the distribution and fragmentation functions we can write the p_T^2-integrated hadron structure functions, normalized by the total cross section, as

$$F_{ep}^h(x, x_B) = \frac{x}{\sigma_{tot}} \frac{d\sigma}{dx}$$

$$= \frac{x}{f_{ep}(x_B)} \left\{ \frac{4}{9}[D_u^h(x)u(x_B) + D_{\bar{u}}^h(x)\bar{u}(x_B)] \right.$$

$$+ \frac{1}{9}[D_d^h(x)d(x_B) + D_{\bar{d}}^h(x)\bar{d}(x_B)]$$

$$\left. + \frac{1}{9}[D_s^h(x)s(x_B) + D_{\bar{s}}^h(x)\bar{s}(x_B)] \right\}.$$ (24)

A similar expression for a neutron target can be obtained by interchanging the constants multiplying the u and d quarks. If we neglect sea-quark contributions,

$$F_{ep}^h(x, x_B) = x \frac{4D_u^h(x)u_v(x_B) + D_d^h(x)d_v(x_B)}{4u_v(x_B) + d_v(x_B)}$$ (25)

F_{ep}^h will be independent of x_B, that is, there will be Feynman scaling, if (i) $u_v(x_B) \gg d_v(x_B)$, (ii) $d_v(x_B) \gg u_v(x_B)$, (iii) u_v and d_v have the same x_B dependence, or (iv) $D_u^h(x) = D_d^h(x)$. From Eqs. (23), (i) and (iii) are only approximately true; (iv) is not indicated by the experiments.[21] We therefore expect Feynman scaling to be only approximately true.

The structure function as a function of x' is also interesting from the point of view of limiting fragmentation.[22] In this model hadrons created in the direction of the virtual photon, $x' > 0$, are considered to be photon fragments whose production is independent of the target. Correspondingly, the hadron fragments produced in the general direction of the target's momentum, $x' < 0$, are considered to be target fragments independent of the photon. For the photon fragmentation region we would expect to find the structure functions independent of the target nucleon. Furthermore, in the vector-meson-dominance (VMD) theory, where the photon has ρ-, ω-, and ϕ-meson-like components, we would expect pions and kaons to be natural fragments of the photon while protons would be suppressed because they are not natural photon fragments. The latter feature is observed in the data.[23-25] For the target fragmentation region we expect to find the structure functions independent of the photon variables. This is seen in the DESY π^- data[26] for real and virtual photoproduction up to $Q^2 \simeq 0.5$ GeV^2, where the structure functions are

consistent with a universal function for $x' < 0$. In the present experiment we do not observe pions with $x' < 0$; the target independence of the structure functions in the photon fragmentation region can, however, be tested.

2. p_T dependence

Most parton models require an upper bound on the transverse momentum so that the impulse approximation and the free-particle field-theory assumptions are valid for the photon-quark interaction. In the Drell, Yan, and Levy[27] model the assumption is made that $Q^2 \gg p_T^2$. Hadron and lepton scattering experiments show that $\langle p_T \rangle$ is small, ~0.5 GeV. No particular Q^2 dependence for $\langle p_T \rangle$ is predicted.

The parton model of Gutbrod and Schröder[28] predicts an increase in $\langle p_T \rangle$ with increasing Q^2. In their model the partons have form factors to account for the nucleon form factors. These form factors cause the inclusive transition matrix element to approach zero with increasing Q^2. To recover the observed scaling of the total cross section, they hypothesize an ever-increasing $\langle p_T \rangle$ as Q^2 increases to just compensate for the decreasing form factors. For $Q^2 \gtrsim 1$ GeV^2, p_T is found to be constant to $Q^2 \sim 20$ GeV^2 in muoproduction and to $Q^2 \sim 60$ GeV^2 in neutrino-production experiments.[29]

In VMD models the photon is considered to be a bare, pointlike photon dressed with vector mesons such as the ρ, ω, and ϕ. For photoproduction and low values of Q^2, VMD predicts the interactions of the fully dressed photon to be apparent. As Q^2 increases and the interaction becomes less peripheral, the pointlike structure of the photon becomes more predominant. This implies a corresponding increase in the average transverse momentum. There is evidence that $\langle p_T \rangle$ initially increases with Q^2 and then becomes Q^2 independent above $Q^2 \simeq M_\rho^2 \simeq 0.5$ GeV^2.[26] This is the point where we would expect the contribution of the photon's ρ nature to be small due to the ρ propagator.

3. ϕ dependence

Ravndal[30] has shown for spin-$\frac{1}{2}$ partons that the azimuthal dependence in Eq. (13) should be small. Experimentally, no significant interference contributions to the cross sections have been observed for $Q^2 \geq 1.2$ GeV^2 in electroproduction experiments[23,31] or for $Q^2 \geq 0.5$ GeV^2 in muoproduction experiments.[32] In the results presented here we assume the interference terms to be zero and average the data over the ϕ range of our acceptance, $0 < \phi < 2\pi$. Equation (13a) is then

$$\frac{d^5\sigma}{dE'd\Omega'd{p_h}^3} = \Gamma\left(\frac{d\sigma_t}{d{p_h}^3} + \epsilon\,\frac{d\sigma_s}{d{p_h}^3}\right) \qquad (26)$$

and the ϕ-averaged structure function is

$$F(x',p_T) = \frac{1}{\pi\sigma_{tot}}\frac{E_h^*}{[(p_{max}^*)^2 - p_T^2]^{1/2}}\frac{d^2\sigma}{dx'dp_T^2} . \qquad (27)$$

B. Charge ratio

The quark-parton model can be extended to predict the charged-pion ratio if we assume factorization of the quark distribution and fragmentation functions as was done above. For the average number of pions from a proton target,

$$\langle n_{\pi^+}\rangle_p \propto \left[\tfrac{4}{9}(D_u^+ u + D_{\bar{u}}^+ \bar{u}) + \tfrac{1}{9}(D_d^+ d + D_{\bar{d}}^+ \bar{d})\right.$$
$$\left. + \tfrac{1}{9}(D_s^+ s + D_{\bar{s}}^+ \bar{s})\right], \qquad (28a)$$

$$\langle n_{\pi^-}\rangle_p \propto \left[\tfrac{4}{9}(D_u^- u + D_{\bar{u}}^- \bar{u}) + \tfrac{1}{9}(D_d^- d + D_{\bar{d}}^- \bar{d})\right.$$
$$\left. + \tfrac{1}{9}(D_s^- s + D_{\bar{s}}^- \bar{s})\right]. \qquad (28b)$$

From isospin and charge-conjugation invariance the

the twelve D's can be reduced to three independent fragmentation functions. Taking the ratio of Eqs. (28), substituting for the parton distribution functions from Eq. (22), and using the reduced D's the charged-pion ratio from protons can be written

$$\frac{\langle n_{\pi^+}\rangle_p}{\langle n_{\pi^-}\rangle_p} = \frac{4\eta(x)u_v(x_B) + d_v(x_B) + [5\eta(x) + 7]c(x_B)}{4u_v(x_B) + \eta(x)d_v(x_B) + [5\eta(x) + 7]c(x_B)} , \qquad (29)$$

where

$$\eta(x) = D_u^+(x)/D_d^+(x) = D_d^-(x)/D_u^-(x) \qquad (30)$$

This is the expression derived by Dakin and Feldman.[33] They further assumed that $\eta(x)$ was a constant; a fit to their data yielded $\eta = 3.0$. The assumption that $\eta(x)$ is a constant is equivalent to the ratio of the π^+ and π^- structure functions being independent of x. The results for neutron and deuteron targets can also be expressed in terms of η,

$$\frac{\langle n_{\pi^+}\rangle_n}{\langle n_{\pi^-}\rangle_n} = \frac{u_v(x_B) + 4\eta(x)d_v(x_B) + [5\eta(x) + 7]c(x_B)}{\eta(x)u_v(x_B) + 4d_v(x_B) + [5\eta(x) + 7]c(x_B)} , \qquad (31)$$

$$\frac{\langle n_{\pi^+}\rangle_d}{\langle n_{\pi^-}\rangle_d} = \frac{(\{4\eta(x)n_v(x_B) + d_v(x_B) + [5\eta(x) + 7]c(x_B)\} + (1 - 0.75x_B)\{u_v(x_B) + 4\eta(x)d_v(x_B) + [5\eta(x) + 7]c(x_B)\})}{(\{4u_v(x_B) + \eta(x)d_v(x_B) + [5\eta(x) + 7]c(x_B)\} + (1 - 0.75x_B)\{\eta(x)u_v(x_B) + 4d_v(x_B) + [5\eta(x) + 7]c(x_B)\})} . \qquad (32)$$

In general, we expect the charge ratio to be a function of x and x_B only, and if η is independent of x, we expect the ratio to be a function of x_B ($= 1/\omega$) only.

In a thermodynamic model such as that of Hagedorn[34] the target nucleon is considered to be excited to energy W by the incident photon and then to radiate hadrons with no charge preference. For a proton we would expect the importance of the initial +1 charge to be diluted with increasing energy and the charge ratio to approach one. For the neutron we would expect the charge ratio to approach unity faster than for the proton since the initial charge state is neutral. In such models the charge ratio is a function of the center-of-mass energy W. In the case of a proton target, given that the charged-particle multiplicity is represented approximately by[35]

$$\langle n\rangle = 1 + 2\ln W , \qquad (33)$$

we might expect the charge ratio to be

$$\frac{\langle n_{\pi^+}\rangle_p}{\langle n_{\pi^-}\rangle_p} = \frac{1 + \ln W}{\ln W} . \qquad (34)$$

The 1 in the numerator reflects the initial +1 charge of the target proton.

C. Scalar-transverse ratio

Because of the nonzero mass of the virtual photon a third polarization state which is along the photon's momentum vector is possible. The contribution of this polarization state to the cross section is a sensitive test for models that assume definite spins for the nucleon constituents. Callan and Gross[36] studied the two cases of spin-$\tfrac{1}{2}$ and spin-1 partons and found that $R = \sigma_s/\sigma_t$ approaches zero or infinity, respectively, as ν goes to infinity. The observed smallness of R in total-cross-section experiments is attributed to spin-$\tfrac{1}{2}$ partons and supports the identification of the partons with quarks.[37,38] From the observed scaling of νW_2 and W_1, Eqs. (21), R should be given by

$$R = Q^2/\nu^2 = 2M/\nu\omega , \qquad (35)$$

showing νR to be a function of ω only. Other parton models predict the same leading ω behavior of νR modified by a function of ω only.[39]

VMD predicts the ratio R to increase with Q^2. In the model of Sakurai,[40] which has the attractive features of predicting the scaling of νW_2 without introducing nucleon constituents and of predicting the right Q^2 dependence of the total cross section, R from protons is given by

$$R = \xi(W)\frac{Q^2}{M_\rho^2}(1 - 1/\omega)^2, \tag{36}$$

where $\xi(W)$ is the ratio of the total ρ nucleon cross sections for longitudinal and transverse polarizations. In recent SLAC results,[37] an increase in R with Q^2 for $\omega \gtrsim 10$ is seen; this is in disagreement with the simple parton model and in agreement with VMD.

By separating the contribution of scalar and transverse photons in a coincidence experiment, we hope to find the source of the scalar part of the total cross section. In the quark-parton picture we expect R in the hadron inclusive spectra to exhibit the same Q^2/ν^2 dependence predicted for the total cross section. Some of the exclusive channels such as $\pi^+ n$ and $K^+\Lambda$ show larger σ_s/σ_t ratios than the total cross section, presumably due to the dominance of meson-exchange diagrams over quark scattering diagrams.[11,41] Harari[42] has proposed that the scalar parts of the exclusive channels account for the entire scalar part of the total cross section. In this paper we will only present a separation for the inclusive pion cross sections.

IV. APPARATUS

The data presented in this paper were taken at the Wilson Electron Synchrotron at Cornell University. The apparatus consisted of two new magnetic spectrometers situated in beam line D. The terminus of the beam line was a lead-tungsten Faraday cup which integrated the incident-beam charge. Figure 3 is a plan view of the apparatus. The tar-
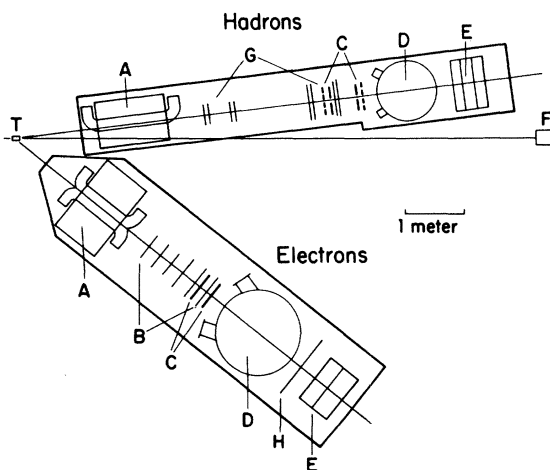

FIG. 3. Plan view of electroproduction apparatus consisting of A: bending magnets, B: spark chambers, C: scintillation counters, D: Freon Čerenkov counters, E: lead-Lucite shower counters, F: Faraday cup, G: multiwire proportional chambers, H: scintillation hodoscope, T: production target.

get, located above the pivot point of the spectrometers, was 12.7 cm long and contained either liquid hydrogen or liquid deuterium.

The hadron spectrometer which was built by the Cornell Large Aperture Spectrometer Group provided hadron vector momentum and particle identification information. It subtended an ~10-msr solid angle. The spectrometer consisted of a vertical bending magnet, four x-y planes of multiwire proportional chambers, and four banks of scintillation counters. Following these was a threshold gas Čerenkov counter which was operated with Freon 12 at 76 psi (absolute) and was used to identify pions. The final counters on the spectrometer were three identical lead-Lucite sandwich shower counters, each approximately four radiation lengths thick. They were used for elastic electron scattering studies and the rejection of electrons during π data taking.

The electron spectrometer was constructed by the Harvard group and had a solid angle of approximately 50 msr. It consisted of a vertical bending magnet followed by six x-y planes of magnetostrictive spark chambers and two planes of scintillation counters. Following these was a gas Čerenkov counter with a $\frac{1}{16}$-in. stainless steel front window. The counter was operated with 22 psi (absolute) of Freon 12. Mounted on the rear of the Čerenkov counter was a six-element vertical hodoscope. The final assemblies of the spectrometer were two identical lead-Lucite sandwich shower counters, each approximately six radiation lengths thick.

The four scintillation counters were used to provide a trigger on the hadron spectrometer. The electron trigger was a coincidence between the two forward scintillators, the Čerenkov counter and the first shower counter. The coincidence of a hadron trigger and an electron defined a recordable event.

To be able to identify hadrons with momenta below the threshold of the hadron Čerenkov counter, two independent time-of-flight measurements were recorded for each event using the second and third scintillators of the hadron spectrometer and the first and second scintillators of the electron spectrometer.

The apparatus was used to collect data at the five nominal kinematic points shown in Table II with hydrogen and deuterium targets. The two significant features of the running points are the large range of Q^2 they span and the low value of the polarization parameter ϵ.

V. ANALYSIS

The analysis of the data consisted of four distinct phases: correction of data events for inefficien-

TABLE II. The nominal kinematic points of the data acquisition.

Data point	Targets	W (GeV)	Q^2 (GeV^2)	ϵ	E (GeV)	θ_e (degrees)	θ_γ (degrees)
1	H_2, D_2	2.15	1.2	0.45	3.59	34.0	11.8
2	H_2, D_2	2.65	2.0	0.35	5.47	34.0	7.6
3	H_2	2.65	3.3	0.40	6.63	34.0	9.3
4	H_2, D_2	2.65	6.2	0.40	8.88	34.0	10.0
5	H_2, D_2	2.65	10.0	0.40	11.21	34.0	8.1

cies and contaminations, a Monte Carlo determination of the apparatus acceptance, absolute calibration of the spectrometers using elastic scattering, and corrections which first required the uncorrected cross sections.

A. Data corrections

The data have been corrected for counter deadtimes [(5 ± 2)%], wire-chamber inefficiencies [(1.5 ± 0.5)%], electron-shower-counter inefficiency [(1 ± 1)%], pion absorption [(5 ± 1)%], hadron-Čerenkov-counter inefficiency and absorption for pions above threshold [(10 ± 2)%], proton contamination due to knock-on events which fired the Čerenkov counter [(5 ± 1)%], and electron contamination of π^- events [(7 ± 1)%]. A correction for the π^- contamination in the electron spectrometer was made according to a subtraction procedure using events known to be pions. The contamination ranged from (3 ± 1)% to (30 ± 3)%. Target-wall events were subtracted from the data using data taken with an empty target. Target-wall events to real events were typically (2 ± 1)%.

Pions were separated from kaons and protons by their time of flight for momenta less than 1.8 GeV and by their pulse height in the Čerenkov counter above 1.8 GeV. Figure 4 shows a sample pion timing spectrum for $0.8 < p_\pi < 1.2$ GeV. The pion peak is Gaussian with a σ of 0.4 nsec; the proton peak is broadened due to the finite-momentum bin. Events within ±1.5 nsec of zero were considered as pions and were corrected for random coincidences and proton misidentification by sampling a region to the right of the proton peak as shown in the figure. Randoms were typically (2 ± 1)% and pion losses due to the timing cut were typically (1 ± 1)%.

B. Monte Carlo acceptance calculation

The Monte Carlo method was used to determine the acceptance of the spectrometers. An electron and a hadron were tossed at the target assuming a unit production cross section. The finite extent of the target and the incident beam were taken into account. The particles were then traced through

the spectrometers while being multiple-scattered through the target, at helium-bag windows, counters, and chambers. At magnet and counter edges, cuts on the physical dimensions of the elements were imposed. Particle trajectories were required to pass through valid trigger-counter combinations. Spark-chamber resolution and proportional-chamber-wire quantization were added to the particle's positions in these chambers and a line finding and fitting procedure simulating the data algorithms was used. Pion decays were simulated to account for losses due to wide-angle muon emission. Monte Carlo events were then reconstructed according to the algorithms applied to the real data events.

C. Normalization

An absolute normalization check for each of the spectrometers was performed using elastic scattering data, $e + p \rightarrow e + p$, acquired by triggering only on a scattered electron. This was done for each data point to check magnet calibrations, surveys, and aperture definitions. An average of the
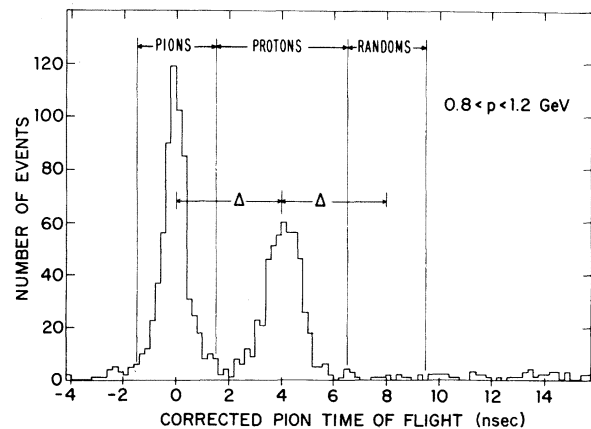

FIG. 4. An example of the pion time-of-flight spectrum for the momentum region $0.8 < p < 1.2$ GeV corrected for length of the particle trajectory, impact point in the counter, and rise time of the photomultiplier pulse. In-time pions lie between −1.5 nsec and 1.5 nsec. Out-of-time pions are sampled from a region centered 2Δ from the in-time peak.

ratio of the measured elastic scattering cross sections to the average of the world data for the electron and hadron arms gave 0.972 ± 0.010 and 0.993 ± 0.004, respectively.

As an added check, data histograms and Monte Carlo histograms, weighted by the elastic scattering cross sections, were compared bin-by-bin for most of the elastic scattering runs at various positions within the spectrometers. This sensitive test for localized discrepancies between the data and the Monte Carlo showed no anomalous behavior in our aperture simulation programs.

D. Dynamics-dependent corrections

1. Neutron separation

The neutron results were found by subtracting the proton results from the deuteron results with the proper normalization taken into account. In the case of the structure function,

$$F_n(x') = \frac{\sigma_d}{\sigma_n} F_d(x') - \frac{\sigma_p}{\sigma_n} F_p(x') . \qquad (37)$$

The total electroproduction cross section, σ_p, with which the structure function was normalized came from a fit to the proton-target results of the SLAC-MIT experiment,[43] assuming $\sigma_s/\sigma_t = 0.18$. The neutron total cross section was assumed to be given by

$$\sigma_n = (1 - 0.75 \, x_B) \sigma_p . \qquad (38)$$

and the deuteron total cross section was assumed to be the simple sum of proton and neutron cross sections,

$$\sigma_d = (2 - 0.75 \, x_B) \sigma_p . \qquad (39)$$

In all kinematics calculations, the target nucleon was assumed to be at rest in the laboratory. For deuterium, the Fermi motion in the nucleus requires a correction for this assumption. A Monte Carlo procedure was used which tossed events according to the structure functions presented later. Each event was tossed first with a stationary target nucleon and then with a moving target nucleon using the Hulthén[44] momentum wave function for deuterium. The kinematics of the latter events were recalculated assuming a stationary nucleon and then compared with the former events to see if any kinematical region was depleted or enhanced by feed-out or feed-in of events. For the plots of the structure function versus x', the change in the structure function at any value of x' was always less than 0.5%, which is less than the estimated error in the calculation. For this reason, the correction was not applied to the data.

Because of the small separation of the two nu-

cleons in the deuteron, it is possible for one nucleon to partially shadow the other nucleon in a geometrical sense. The effect is to reduce the effective number of nucleons that can interact with an incident electron. The effect appears as a cross-section defect[45]

$$\delta\sigma = \sigma_p + \sigma_n - \sigma_d . \qquad (40)$$

The defect is estimated to be less than 0.1% for the kinematic regions of this experiment.

2. Radiative correction

One of the major and most difficult to calculate corrections to electroproduction data is the radiative correction. The radiation of energy by the electrons introduces an error into all calculations of the electron kinematic variables, W, Q^2, ϵ, and also affects any hadron variable calculated relative to the virtual photon whose direction and energy will not be as assumed. A procedure similar to the deuteron Fermi-motion study was used to determine how radiative events redistributed themselves. In particular, the structure function as a function of x' was studied. Electrons were tossed at fixed values of W, Q^2, and ϵ and hadrons were tossed according to x' distributions measured from the data. The tossed electron was allowed to radiate following the procedure of Mo and Tsai[46] and Γ, σ_{tot}, and the new hadron kinematics were recalculated. By comparing the number of events tossed at any x' with the number of events that reconstructed to that x' an estimate of the radiative correction could be made.

The ranges of W and Q^2 at which real reactions occur and contribute to an observed W and Q^2 are very broad. Knowledge of the electroproduction cross section over this entire range is required if events which feed into a given bin are to be properly weighted. The inclusive cross section over the W and Q^2 range required is not known, especially at low values of W and Q^2, where scaling does not work. Because of this, no radiative corrections have been applied to the data. Some general observations about the correction could be made, however. The shape of the structure function versus x' was not changed very much. To first order, the correction simply scaled the structure function by roughly 1.15 for $0 < x' < 0.8$. The exact number varied by $\pm 5\%$ among the various (W, Q^2, ϵ) points. In Tables III to VI the radiative correction factor has been included in one column; $F(x')$ itself is not corrected.

E. Systematic uncertainty

The errors on the results presented in the figures and the tables reflect only the data and Monte

TABLE III. The π^+ structure function from hydrogen and kinematic averages for $p_T^2 < 0.02$ GeV^2 as a function of x' (bin size is 0.05). Rad. corr. is an estimate of the radiative correction but is not applied to $F(x')$. N is the number of events in the bin.

x'	$F(x')$ (GeV^{-2})	W (GeV)	Q^2 (GeV^2)	ϵ	p_T^2 (GeV^2)	ω	σ_p (μb)	Rad. corr.	N
			(a) $W = 2.2$ GeV, $Q^2 = 1.2$ GeV^2						
0.078	0.544 ± 0.464	2.23	1.02	0.39	0.0001	5.02	46.56	1.008	5
0.134	0.627 ± 0.243	2.10	1.20	0.47	0.0011	3.98	43.39	1.043	19
0.176	1.090 ± 0.204	2.14	1.16	0.44	0.0015	4.26	43.79	1.027	64
0.227	0.797 ± 0.150	2.16	1.15	0.43	0.0020	4.32	43.64	1.073	85
0.276	0.826 ± 0.105	2.12	1.19	0.45	0.0024	4.11	43.54	1.083	133
0.327	0.809 ± 0.084	2.11	1.18	0.46	0.0031	4.11	43.70	1.051	162
0.376	0.626 ± 0.066	2.13	1.18	0.44	0.0050	4.16	43.35	1.093	168
0.425	0.515 ± 0.045	2.13	1.17	0.45	0.0054	4.19	43.75	1.087	208
0.476	0.417 ± 0.038	2.13	1.18	0.45	0.0065	4.15	43.58	1.107	203
0.525	0.416 ± 0.033	2.12	1.18	0.45	0.0065	4.11	43.51	1.107	258
0.576	0.319 ± 0.027	2.12	1.17	0.46	0.0075	4.13	43.86	1.116	230
0.626	0.341 ± 0.028	2.12	1.17	0.45	0.0071	4.16	43.85	1.114	266
0.675	0.207 ± 0.022	2.12	1.18	0.45	0.0075	4.11	43.51	1.110	199
0.726	0.237 ± 0.020	2.12	1.17	0.46	0.0086	4.14	43.98	1.126	229
0.774	0.298 ± 0.022	2.10	1.20	0.47	0.0081	3.99	43.43	1.123	283
0.825	0.337 ± 0.022	2.11	1.20	0.46	0.0076	4.03	43.31	1.152	334
0.872	0.227 ± 0.018	2.11	1.20	0.46	0.0081	4.04	43.17	1.197	224
0.925	0.151 ± 0.016	2.11	1.20	0.45	0.0087	4.03	43.23	1.224	154
0.986	0.776 ± 0.036	2.11	1.19	0.46	0.0082	4.04	43.60	1.339	745
1.009	0.583 ± 0.032	2.10	1.20	0.47	0.0087	3.99	43.54	1.339	546
1.076	0.014 ± 0.005	2.03	1.18	0.50	0.0077	3.76	45.28	1.339	13
			(b) $W = 2.7$ GeV, $Q^2 = 2.0$ GeV^2						
0.037	1.357 ± 0.603	2.66	2.06	0.33	0.0007	4.05	23.57	0.993	7
0.080	1.357 ± 0.329	2.64	2.02	0.35	0.0005	4.07	24.18	1.008	38
0.123	0.782 ± 0.198	2.68	1.96	0.33	0.0015	4.30	24.69	1.043	59
0.174	1.160 ± 0.131	2.68	1.91	0.33	0.0013	4.38	25.28	1.027	152
0.225	0.919 ± 0.104	2.67	1.93	0.33	0.0022	4.32	24.98	1.073	171
0.276	0.604 ± 0.068	2.67	1.94	0.33	0.0036	4.30	25.02	1.083	170
0.326	0.592 ± 0.052	2.66	1.95	0.34	0.0054	4.25	24.90	1.051	236
0.375	0.473 ± 0.040	2.66	1.97	0.33	0.0065	4.22	24.66	1.093	286
0.426	0.403 ± 0.031	2.67	1.95	0.33	0.0068	4.26	24.82	1.087	316
0.475	0.369 ± 0.025	2.67	1.95	0.33	0.0066	4.27	24.77	1.107	357
0.523	0.314 ± 0.022	2.67	1.94	0.34	0.0075	4.29	25.00	1.107	338
0.574	0.267 ± 0.020	2.65	1.98	0.34	0.0075	4.18	24.65	1.116	308
0.623	0.252 ± 0.019	2.66	1.96	0.34	0.0081	4.22	24.75	1.114	308
0.675	0.228 ± 0.018	2.65	1.97	0.34	0.0076	4.20	24.74	1.110	279
0.725	0.203 ± 0.016	2.65	1.97	0.34	0.0089	4.19	24.71	1.126	250
0.774	0.171 ± 0.015	2.66	1.95	0.34	0.0084	4.23	24.85	1.123	207
0.826	0.124 ± 0.013	2.66	1.97	0.34	0.0098	4.22	24.73	1.152	149
0.876	0.138 ± 0.014	2.64	1.99	0.34	0.0091	4.12	24.49	1.197	157
0.922	0.143 ± 0.014	2.66	1.95	0.34	0.0093	4.23	24.85	1.224	152
0.986	0.242 ± 0.018	2.65	1.99	0.35	0.0083	4.13	24.54	1.339	263
1.010	0.266 ± 0.022	2.64	1.98	0.34	0.0084	4.14	24.61	1.339	249
			(c) $W = 2.7$ GeV, $Q^2 = 3.3$ GeV^2						
0.036	1.034 ± 0.382	2.65	3.33	0.38	0.0006	2.91	14.46	0.993	12
0.081	1.238 ± 0.232	2.70	3.22	0.36	0.0015	3.04	14.95	1.008	60
0.129	1.245 ± 0.144	2.69	3.21	0.37	0.0019	3.04	15.01	1.043	144
0.176	1.035 ± 0.091	2.67	3.24	0.38	0.0032	2.98	14.85	1.027	196
0.228	0.837 ± 0.071	2.67	3.25	0.38	0.0051	2.96	14.80	1.073	229
0.275	0.701 ± 0.060	2.67	3.23	0.38	0.0060	2.98	14.90	1.083	241
0.325	0.603 ± 0.055	2.67	3.22	0.38	0.0064	2.98	14.93	1.051	244
0.375	0.505 ± 0.044	2.68	3.25	0.38	0.0081	2.98	14.80	1.093	242
0.426	0.434 ± 0.036	2.68	3.22	0.38	0.0086	2.99	14.96	1.087	250

TABLE III. (*Continued*)

x'	$F(x')$ (GeV^{-2})	W (GeV)	Q^2 (GeV^2)	ϵ	p_T^2 (GeV^2)	ω	σ_p (μb)	Rad. corr.	N
0.475	0.431 ± 0.032	2.66	3.28	0.38	0.0091	2.93	14.60	1.107	301
0.526	0.307 ± 0.026	2.65	3.30	0.38	0.0085	2.91	14.56	1.107	253
0.576	0.309 ± 0.023	2.65	3.31	0.38	0.0087	2.90	14.46	1.116	289
0.623	0.214 ± 0.021	2.63	3.37	0.39	0.0084	2.83	14.13	1.114	204
0.673	0.269 ± 0.022	2.65	3.31	0.38	0.0086	2.90	14.48	1.110	260
0.722	0.198 ± 0.018	2.67	3.27	0.38	0.0096	2.95	14.69	1.126	189
0.773	0.170 ± 0.018	2.67	3.23	0.38	0.0099	2.98	14.94	1.123	163
0.822	0.150 ± 0.016	2.63	3.36	0.39	0.0090	2.84	14.22	1.152	136
0.875	0.150 ± 0.016	2.63	3.36	0.39	0.0087	2.83	14.20	1.197	124
0.921	0.128 ± 0.016	2.64	3.32	0.39	0.0098	2.88	14.44	1.224	105
0.987	0.240 ± 0.023	2.64	3.35	0.39	0.0101	2.86	14.24	1.339	180
1.007	0.205 ± 0.022	2.62	3.36	0.40	0.0093	2.82	14.23	1.339	148

(d) $W = 2.7$ GeV, $Q^2 = 6.2$ GeV^2

x'	$F(x')$ (GeV^{-2})	W (GeV)	Q^2 (GeV^2)	ϵ	p_T^2 (GeV^2)	ω	σ_p (μb)	Rad. corr.	N
0.032	1.755 ± 0.716	2.63	6.27	0.42	0.0015	1.97	5.59	0.993	15
0.077	1.159 ± 0.353	2.67	6.16	0.40	0.0009	2.04	5.88	1.008	30
0.128	1.264 ± 0.231	2.68	6.24	0.39	0.0031	2.03	5.75	1.043	64
0.175	0.942 ± 0.168	2.65	6.25	0.41	0.0059	2.00	5.68	1.027	75
0.221	0.710 ± 0.143	2.73	6.08	0.39	0.0060	2.10	6.13	1.073	76
0.277	0.535 ± 0.113	2.73	6.02	0.39	0.0089	2.11	6.27	1.083	67
0.326	0.711 ± 0.101	2.72	6.15	0.39	0.0094	2.08	6.01	1.051	105
0.379	0.478 ± 0.083	2.70	6.11	0.40	0.0095	2.07	6.04	1.093	86
0.425	0.386 ± 0.068	2.72	6.11	0.39	0.0087	2.08	6.05	1.087	81
0.474	0.399 ± 0.062	2.69	6.20	0.39	0.0077	2.04	5.84	1.107	95
0.525	0.284 ± 0.054	2.64	6.28	0.41	0.0086	1.99	5.64	1.107	68
0.576	0.274 ± 0.054	2.64	6.21	0.42	0.0088	2.00	5.76	1.116	62
0.629	0.189 ± 0.046	2.72	5.93	0.41	0.0098	2.11	6.34	1.114	42
0.682	0.160 ± 0.039	2.74	6.00	0.39	0.0101	2.12	6.30	1.110	37
0.725	0.152 ± 0.040	2.64	6.29	0.42	0.0095	1.98	5.61	1.126	32
0.777	0.211 ± 0.043	2.70	6.15	0.40	0.0107	2.05	5.92	1.123	41
0.821	0.120 ± 0.036	2.65	6.38	0.40	0.0069	1.98	5.51	1.152	21
0.854	0.056 ± 0.034	2.65	6.11	0.42	0.0048	2.03	5.94	1.197	9
0.924	0.200 ± 0.047	2.63	6.47	0.40	0.0072	1.96	5.34	1.224	31
0.987	0.200 ± 0.048	2.70	6.15	0.40	0.0017	2.06	5.94	1.339	29
1.008	0.172 ± 0.044	2.68	6.29	0.39	0.0105	2.02	5.71	1.339	25

(e) $W = 2.7$ GeV, $Q^2 = 9.5$ GeV^2

x'	$F(x')$ (GeV^{-2})	W (GeV)	Q^2 (GeV^2)	ϵ	p_T^2 (GeV^2)	ω	σ_p (μb)	Rad. corr.	N
0.028	1.306 ± 0.476	2.68	9.60	0.40	0.0023	1.66	2.49	0.993	12
0.075	1.169 ± 0.295	2.73	9.57	0.38	0.0035	1.69	2.60	1.008	29
0.127	1.259 ± 0.205	2.70	9.52	0.39	0.0041	1.68	2.59	1.043	56
0.179	0.915 ± 0.164	2.72	9.51	0.39	0.0063	1.69	2.62	1.027	58
0.226	1.049 ± 0.150	2.68	9.60	0.39	0.0074	1.66	2.50	1.073	81
0.277	0.603 ± 0.100	2.68	9.67	0.39	0.0100	1.66	2.47	1.083	70
0.324	0.633 ± 0.085	2.68	9.63	0.39	0.0078	1.66	2.48	1.051	95
0.377	0.446 ± 0.068	2.70	9.47	0.39	0.0089	1.69	2.61	1.093	78
0.421	0.439 ± 0.064	2.68	9.59	0.39	0.0081	1.66	2.51	1.087	83
0.474	0.268 ± 0.053	2.64	9.77	0.40	0.0085	1.63	2.34	1.107	48
0.530	0.261 ± 0.056	2.72	9.51	0.38	0.0102	1.70	2.63	1.107	46
0.575	0.304 ± 0.059	2.69	9.66	0.39	0.0107	1.66	2.47	1.116	48
0.617	0.311 ± 0.063	2.65	9.63	0.40	0.0101	1.65	2.45	1.114	43
0.671	0.145 ± 0.052	2.66	9.53	0.40	0.0107	1.66	2.52	1.110	20
0.731	0.256 ± 0.056	2.71	9.48	0.39	0.0099	1.69	2.63	1.126	35
0.769	0.135 ± 0.042	2.73	9.27	0.40	0.0100	1.72	2.80	1.123	17
0.818	0.106 ± 0.040	2.68	9.64	0.39	0.0099	1.66	2.47	1.152	12
0.873	0.077 ± 0.037	2.61	9.65	0.42	0.0097	1.62	2.34	1.197	7
0.928	0.162 ± 0.047	2.70	9.31	0.41	0.0077	1.69	2.70	1.224	18
0.987	0.232 ± 0.073	2.64	9.87	0.39	0.0097	1.62	2.28	1.339	19
1.010	0.243 ± 0.086	2.58	9.84	0.42	0.0090	1.59	2.21	1.339	14

TABLE IV. The π^- structure function from hydrogen and kinematic averages for $p_T^2 < 0.02$ GeV^2 as a function of x' (bin size is 0.05). Rad. corr. is an estimate of the radiative correction but is not applied to $F(x')$. N is the number of events in the bin.

x'	$F(x')$ (GeV^{-2})	W (GeV)	Q^2 (GeV^2)	ϵ	p_T^2 (GeV^2)	ω	σ_p (μb)	Rad. corr.	N
			(a) $W = 2.2$ GeV, $Q^2 = 1.2$ GeV^2						
0.122	0.799 ± 0.195	2.12	1.19	0.46	0.0009	4.10	43.58	1.055	25
0.173	0.801 ± 0.147	2.12	1.17	0.45	0.0012	4.13	43.79	1.040	47
0.225	0.717 ± 0.113	2.10	1.20	0.46	0.0019	4.03	43.39	1.088	75
0.275	0.497 ± 0.065	2.11	1.18	0.46	0.0024	4.10	43.80	1.100	78
0.325	0.447 ± 0.055	2.11	1.19	0.46	0.0026	4.05	43.53	1.068	86
0.376	0.278 ± 0.042	2.13	1.19	0.44	0.0046	4.13	43.31	1.112	69
0.426	0.224 ± 0.033	2.11	1.17	0.46	0.0059	4.11	44.26	1.106	79
0.475	0.255 ± 0.031	2.12	1.19.	0.45	0.0066	4.10	43.50	1.127	105
0.526	0.193 ± 0.022	2.12	1.18	0.45	0.0071	4.12	43.72	1.127	99
0.576	0.188 ± 0.020	2.12	1.18	0.45	0.0067	4.12	43.52	1.137	110
0.624	0.187 ± 0.020	2.11	1.19	0.46	0.0075	4.06	43.67	1.134	116
0.675	0.177 ± 0.019	2.12	1.17	0.45	0.0074	4.14	43.93	1.129	133
0.726	0.153 ± 0.019	2.12	1.17	0.46	0.0082	4.14	43.99	1.145	116
0.776	0.260 ± 0.023	2.09	1.21	0.47	0.0062	3.90	43.36	1.141	192
0.825	0.297 ± 0.024	2.10	1.20	0.47	0.0076	3.99	43.50	1.169	227
0.872	0.204 ± 0.019	2.11	1.17	0.46	0.0086	4.10	43.90	1.212	155
0.911	0.040 ± 0.008	2.12	1.18	0.46	0.0084	4.11	43.68	1.235	32
0.998	0.004 ± 0.003	1.96	1.43	0.54	0.0144	3.02	39.76	1.343	3
			(b) $W = 2.7$ GeV, $Q^2 = 2.0$ GeV^2						
0.019	0.426 ± 0.629	2.66	1.95	0.34	0.0012	4.29	24.82	1.002	3
0.080	0.889 ± 0.198	2.71	1.84	0.31	0.0005	4.55	25.73	1.018	34
0.124	0.935 ± 0.128	2.66	1.98	0.33	0.0011	4.19	24.47	1.055	96
0.177	0.641 ± 0.079	2.65	1.98	0.35	0.0015	4.15	24.59	1.040	112
0.227	0.477 ± 0.058	2.66	1.95	0.33	0.0023	4.27	24.91	1.088	116
0.276	0.534 ± 0.049	2.66	1.97	0.33	0.0034	4.23	24.68	1.100	186
0.328	0.382 ± 0.036	2.68	1.93	0.33	0.0049	4.33	25.05	1.068	170
0.376	0.365 ± 0.031	2.65	1.98	0.34	0.0059	4.16	24.60	1.112	207
0.425	0.239 ± 0.024	2.65	1.96	0.34	0.0063	4.22	24.77	1.106	160
0.473	0.195 ± 0.022	2.66	1.98	0.33	0.0072	4.20	24.56	1.127	148
0.524	0.136 ± 0.017	2.65	1.98	0.34	0.0072	4.17	24.64	1.127	109
0.572	0.151 ± 0.017	2.66	1.97	0.34	0.0072	4.21	24.62	1.137	125
0.625	0.095 ± 0.013	2.65	1.98	0.34	0.0100	4.18	24.56	1.134	80
0.672	0.103 ± 0.014	2.66	1.98	0.34	0.0091	4.19	24.60	1.129	86
0.723	0.080 ± 0.012	2.65	1.96	0.34	0.0075	4.20	24.86	1.145	66
0.774	0.088 ± 0.013	2.65	1.99	0.34	0.0083	4.16	24.54	1.141	71
0.828	0.090 ± 0.013	2.64	2.00	0.35	0.0083	4.12	24.45	1.169	73
0.877	0.113 ± 0.014	2.66	1.95	0.34	0.0091	4.23	24.90	1.212	85
0.916	0.076 ± 0.013	2.68	1.91	0.33	0.0087	4.34	25.30	1.235	51
0.953	0.002 ± 0.002	2.63	1.87	0.36	0.0057	4.23	25.99	1.343	1
			(c) $W = 2.7$ GeV, $Q^2 = 3.3$ GeV^2						
0.028	0.787 ± 0.389	2.65	3.13	0.41	0.0006	2.98	15.45	1.002	9
0.075	1.073 ± 0.205	2.69	3.21	0.37	0.0011	3.02	14.98	1.018	45
0.128	0.773 ± 0.109	2.67	3.23	0.38	0.0025	2.99	14.92	1.055	79
0.174	0.786 ± 0.080	2.69	3.20	0.37	0.0036	3.05	15.03	1.040	143
0.227	0.531 ± 0.052	2.68	3.22	0.37	0.0054	3.01	14.97	1.088	147
0.276	0.396 ± 0.039	2.68	3.21	0.37	0.0063	3.01	14.99	1.100	137
0.326	0.326 ± 0.035	2.70	3.19	0.37	0.0066	3.05	15.12	1.068	134
0.378	0.311 ± 0.033	2.66	3.28	0.38	0.0083	2.94	14.63	1.112	142
0.426	0.234 ± 0.027	2.66	3.25	0.38	0.0087	2.95	14.78	1.106	118
0.473	0.209 ± 0.025	2.63	3.37	0.39	0.0088	2.84	14.17	1.127	114
0.524	0.195 ± 0.021	2.66	3.26	0.38	0.0087	2.94	14.74	1.127	117
0.577	0.090 ± 0.016	2.67	3.22	0.38	0.0093	2.99	15.02	1.137	56
0.627	0.075 ± 0.014	2.66	3.32	0.38	0.0080	2.90	14.37	1.134	48

TABLE IV. (*Continued*)

x'	$F(x')$ (GeV^{-2})	W (GeV)	Q^2 (GeV^2)	ϵ	p_T^2 (GeV^2)	ω	σ_p (μb)	Rad. corr.	N
0.676	0.077 ± 0.014	2.68	3.23	0.38	0.0099	2.98	14.90	1.129	49
0.721	0.054 ± 0.011	2.65	3.30	0.39	0.0091	2.90	14.50	1.145	33
0.773	0.065 ± 0.013	2.65	3.30	0.39	0.0076	2.91	14.60	1.141	38
0.822	0.084 ± 0.014	2.63	3.31	0.40	0.0091	2.86	14.47	1.169	49
0.877	0.106 ± 0.018	2.65	3.31	0.38	0.0098	2.90	14.47	1.212	54
0.918	0.070 ± 0.014	2.65	3.30	0.39	0.0095	2.90	14.53	1.235	36
0.954	0.009 ± 0.006	2.72	3.15	0.36	0.0160	3.09	15.31	1.343	4

(d) $W = 2.7$ GeV, $Q^2 = 6.2$ GeV^2

x'	$F(x')$ (GeV^{-2})	W (GeV)	Q^2 (GeV^2)	ϵ	p_T^2 (GeV^2)	ω	σ_p (μb)	Rad. corr.	N
0.035	0.850 ± 0.479	2.58	6.34	0.42	0.0007	1.93	5.38	1.002	9
0.077	0.797 ± 0.239	2.72	6.16	0.38	0.0016	2.07	5.93	1.018	24
0.128	0.824 ± 0.159	2.71	6.06	0.39	0.0052	2.09	6.14	1.055	49
0.175	0.848 ± 0.119	2.69	6.17	0.40	0.0055	2.05	5.90	1.040	78
0.225	0.601 ± 0.086	2.68	6.15	0.40	0.0062	2.04	5.91	1.088	73
0.275	0.461 ± 0.073	2.66	6.24	0.39	0.0067	2.02	5.74	1.100	64
0.325	0.312 ± 0.060	2.70	6.06	0.39	0.0085	2.08	6.13	1.068	47
0.376	0.223 ± 0.052	2.67	6.25	0.40	0.0079	2.02	5.75	1.112	37
0.428	0.166 ± 0.044	2.71	6.24	0.38	0.0058	2.06	5.83	1.106	28
0.475	0.239 ± 0.045	2.69	6.27	0.39	0.0079	2.03	5.74	1.127	44
0.523	0.109 ± 0.033	2.69	6.27	0.39	0.0062	2.03	5.75	1.127	20
0.578	0.116 ± 0.031	2.71	6.02	0.40	0.0105	2.09	6.20	1.137	20
0.620	0.088 ± 0.033	2.65	6.29	0.40	0.0092	2.00	5.66	1.134	14
0.669	0.059 ± 0.028	2.75	5.71	0.41	0.0098	2.19	6.89	1.129	10
0.723	0.061 ± 0.023	2.68	6.02	0.41	0.0079	2.06	6.13	1.145	9
0.781	0.034 ± 0.018	2.72	6.11	0.38	0.0107	2.07	6.01	1.141	5
0.822	0.043 ± 0.022	2.68	6.29	0.39	0.0135	2.02	5.69	1.169	5
0.875	0.115 ± 0.041	2.71	6.25	0.38	0.0125	2.05	5.79	1.212	13
0.920	0.037 ± 0.022	2.75	5.80	0.41	0.0087	2.16	6.67	1.235	4

(e) $W = 2.7$ GeV, $Q^2 = 9.5$ GeV^2

x'	$F(x')$ (GeV^{-2})	W (GeV)	Q^2 (GeV^2)	ϵ	p_T^2 (GeV^2)	ω	σ_p (μb)	Rad. corr.	N
0.065	1.033 ± 0.516	2.69	9.50	0.39	0.0027	1.67	2.54	1.018	23
0.129	0.629 ± 0.161	2.68	9.59	0.39	0.0033	1.66	2.49	1.055	26
0.177	0.678 ± 0.125	2.73	9.48	0.38	0.0057	1.71	2.67	1.040	40
0.216	0.308 ± 0.092	2.75	9.35	0.38	0.0070	1.73	2.77	1.088	21
0.277	0.332 ± 0.080	2.68	9.56	0.39	0.0082	1.67	2.53	1.100	30
0.323	0.214 ± 0.058	2.79	9.20	0.37	0.0058	1.76	2.91	1.068	22
0.373	0.218 ± 0.056	2.74	9.45	0.38	0.0088	1.71	2.69	1.112	24
0.425	0.116 ± 0.050	2.56	10.21	0.40	0.0091	1.55	1.90	1.106	14
0.482	0.113 ± 0.044	2.72	9.34	0.39	0.0107	1.71	2.76	1.127	12
0.527	0.088 ± 0.037	2.86	9.16	0.35	0.0064	1.79	3.02	1.127	9
0.571	0.090 ± 0.037	2.75	9.07	0.41	0.0124	1.74	2.94	1.137	8
0.632	0.044 ± 0.029	2.71	9.60	0.37	0.0144	1.70	2.65	1.134	4
0.660	0.186 ± 0.153	2.86	9.23	0.34	0.0078	1.79	2.98	1.129	15
0.725	0.054 ± 0.031	2.71	9.75	0.36	0.0130	1.67	2.46	1.145	4
0.835	0.044 ± 0.032	2.53	9.80	0.44	0.0076	1.57	2.14	1.169	3
0.869	0.028 ± 0.028	2.51	9.92	0.44	0.0136	1.55	2.02	1.212	1
0.908	0.024 ± 0.024	2.68	9.38	0.41	0.0028	1.67	2.60	1.235	1

Carlo statistical errors. In addition to these, there are the errors from the uncertainties in the corrections applied to the data and the uncertainty in the absolute normalization check. It is estimated that the residual systematic uncertainty is ±7.5%.

F. W, Q^2 binning

All the data presented in this paper have been cut on W and Q^2 to reduce the correlations between W, Q^2, and x'. The W bins extended ±0.25 GeV from the nominal W values listed in Table II. The

TABLE V. The π^+ structure function from deuterium and kinematic averages for $p_T{}^2 < 0.02$ GeV^2 as a function of x' (bin size is 0.05). The total cross section is for a proton target. Rad. corr. is an estimate of the radiative corrections but is not applied to $F(x')$. N is the number of events in the bin.

x'	$F(x')$ (GeV^{-2})	W (GeV)	Q^2 (GeV^2)	ϵ	$p_T{}^2$ (GeV^2)	ω	σ_p (μb)	Rad. corr.	N
(a) $W = 2.2$ GeV, $Q^2 = 1.2$ GeV^2
0.046	1.478 ± 1.682	2.26	1.04	0.36	0.0010	5.06	45.08	0.993	1
0.079	1.041 ± 0.297	2.15	1.14	0.43	0.0006	4.34	44.06	1.008	21
0.127	0.930 ± 0.183	2.12	1.19	0.45	0.0005	4.10	43.25	1.043	59
0.172	1.112 ± 0.143	2.12	1.19	0.45	0.0012	4.10	43.36	1.027	133
0.226	0.514 ± 0.102	2.12	1.19	0.45	0.0018	4.10	43.33	1.073	109
0.273	0.508 ± 0.069	2.11	1.22	0.46	0.0019	3.99	42.80	1.083	162
0.326	0.518 ± 0.062	2.13	1.18	0.44	0.0029	4.17	43.53	1.051	204
0.375	0.479 ± 0.047	2.13	1.18	0.44	0.0047	4.17	43.39	1.093	243
0.426	0.342 ± 0.033	2.12	1.18	0.45	0.0053	4.14	43.60	1.087	244
0.474	0.377 ± 0.030	2.12	1.19	0.45	0.0059	4.08	43.54	1.107	310
0.525	0.322 ± 0.023	2.12	1.18	0.45	0.0072	4.11	43.54	1.107	330
0.574	0.276 ± 0.021	2.11	1.19	0.46	0.0065	4.08	43.58	1.116	323
0.624	0.254 ± 0.020	2.13	1.17	0.45	0.0077	4.18	43.76	1.114	314
0.676	0.221 ± 0.019	2.11	1.18	0.46	0.0075	4.08	43.65	1.110	331
0.725	0.245 ± 0.017	2.10	1.20	0.46	0.0075	4.02	43.43	1.126	366
0.777	0.325 ± 0.019	2.10	1.19	0.47	0.0081	4.03	43.66	1.123	474
0.826	0.342 ± 0.019	2.11	1.19	0.46	0.0079	4.08	43.50	1.152	516
0.872	0.284 ± 0.017	2.12	1.18	0.45	0.0078	4.14	43.65	1.197	426
0.925	0.130 ± 0.013	2.11	1.19	0.46	0.0090	4.04	43.65	1.224	202
0.983	0.331 ± 0.019	2.11	1.20	0.46	0.0083	4.01	43.25	1.339	474
1.011	0.313 ± 0.019	2.10	1.21	0.47	0.0084	3.95	43.28	1.339	439
1.069	0.004 ± 0.002	2.06	1.30	0.49	0.0068	3.60	41.51	1.339	5
(b) $W = 2.7$ GeV, $Q^2 = 2.0$ GeV^2
0.038	1.553 ± 0.546	2.69	1.93	0.32	0.0003	4.36	24.94	0.993	16
0.077	2.086 ± 0.263	2.69	1.92	0.32	0.0006	4.38	25.03	1.008	117
0.126	0.698 ± 0.151	2.65	1.98	0.34	0.0010	4.18	24.54	1.043	99
0.179	0.895 ± 0.104	2.66	1.97	0.34	0.0015	4.22	24.66	1.027	211
0.225	0.854 ± 0.082	2.66	1.96	0.34	0.0023	4.24	24.78	1.073	276
0.276	0.619 ± 0.056	2.68	1.91	0.33	0.0039	4.39	25.24	1.083	290
0.326	0.466 ± 0.041	2.66	1.98	0.34	0.0056	4.18	24.55	1.051	303
0.375	0.432 ± 0.032	2.68	1.93	0.33	0.0060	4.32	25.06	1.093	424
0.425	0.381 ± 0.025	2.66	1.96	0.34	0.0069	4.23	24.76	1.087	481
0.475	0.298 ± 0.019	2.66	1.97	0.34	0.0073	4.22	24.66	1.107	465
0.525	0.273 ± 0.017	2.66	1.96	0.34	0.0072	4.24	24.75	1.107	473
0.575	0.251 ± 0.016	2.66	1.95	0.34	0.0077	4.23	24.86	1.116	466
0.624	0.218 ± 0.014	2.66	1.96	0.34	0.0077	4.23	24.79	1.114	432
0.676	0.176 ± 0.013	2.66	1.96	0.34	0.0083	4.22	24.77	1.110	347
0.725	0.154 ± 0.012	2.65	1.97	0.35	0.0082	4.18	24.80	1.126	305
0.773	0.140 ± 0.011	2.66	1.95	0.34	0.0085	4.25	24.91	1.123	274
0.824	0.137 ± 0.011	2.65	1.99	0.35	0.0090	4.15	24.57	1.152	263
0.877	0.181 ± 0.013	2.65	1.99	0.34	0.0085	4.13	24.53	1.197	332
0.920	0.164 ± 0.012	2.66	1.97	0.34	0.0083	4.19	24.68	1.224	283
0.984	0.154 ± 0.012	2.65	1.99	0.34	0.0089	4.15	24.51	1.339	271
1.008	0.127 ± 0.012	2.65	1.97	0.34	0.0093	4.18	24.68	1.339	191
1.094	0.001 ± 0.002	2.69	1.89	0.34	0.0018	4.30	25.27	1.339	2
(c) $W = 2.7$ GeV, $Q^2 = 6.2$ GeV^2
0.016	0.831 ± 0.533	2.63	6.39	0.39	0.0011	1.93	5.25	0.993	13
0.074	1.388 ± 0.270	2.66	6.24	0.41	0.0018	2.01	5.73	1.008	67
0.129	0.735 ± 0.156	2.70	6.15	0.40	0.0025	2.06	5.97	1.043	69
0.178	0.809 ± 0.121	2.69	6.18	0.40	0.0041	2.05	5.90	1.027	119
0.222	0.624 ± 0.099	2.69	6.16	0.40	0.0072	2.05	5.94	1.073	122
0.275	0.608 ± 0.086	2.72	6.00	0.40	0.0069	2.10	6.24	1.083	137

TABLE V. (*Continued*)

x'	$F(x')$ (GeV^{-2})	W (GeV)	Q^2 (GeV^2)	ϵ	p_T^2 (GeV^2)	ω	σ_p (μb)	Rad. corr.	N
0.327	0.597 ± 0.074	2.71	6.10	0.40	0.0094	2.08	6.08	1.051	148
0.371	0.405 ± 0.062	2.71	6.05	0.40	0.0085	2.08	6.14	1.093	112
0.423	0.338 ± 0.059	2.67	6.27	0.40	0.0075	2.02	5.71	1.087	98
0.478	0.308 ± 0.051	2.67	6.13	0.41	0.0096	2.04	5.95	1.107	98
0.529	0.277 ± 0.047	2.67	6.15	0.41	0.0083	2.03	5.89	1.107	86
0.577	0.314 ± 0.049	2.65	6.27	0.41	0.0099	1.99	5.63	1.116	92
0.623	0.187 ± 0.042	2.72	5.98	0.40	0.0095	2.11	6.29	1.114	52
0.676	0.199 ± 0.037	2.69	6.17	0.40	0.0088	2.04	5.90	1.110	57
0.723	0.140 ± 0.036	2.63	6.26	0.41	0.0076	1.98	5.63	1.126	36
0.776	0.127 ± 0.033	2.70	6.11	0.40	0.0099	2.07	6.05	1.123	30
0.828	0.089 ± 0.032	2.64	6.24	0.42	0.0108	1.98	5.65	1.152	19
0.871	0.107 ± 0.032	2.60	6.44	0.42	0.0060	1.94	5.33	1.197	21
0.922	0.164 ± 0.037	2.66	6.26	0.40	0.0085	2.01	5.71	1.224	31
0.986	0.101 ± 0.032	2.69	6.07	0.40	0.0076	2.07	6.10	1.339	17
1.012	0.077 ± 0.028	2.62	6.32	0.42	0.0089	1.96	5.51	1.339	13

(d) $W = 2.7$ GeV, $Q^2 = 9.5$ GeV^2

x'	$F(x')$ (GeV^{-2})	W (GeV)	Q^2 (GeV^2)	ϵ	p_T^2 (GeV^2)	ω	σ_p (μb)	Rad. corr.	N
0.027	0.866 ± 0.605	2.78	9.28	0.38	0.0008	1.74	2.82	0.993	6
0.074	1.333 ± 0.347	2.75	9.09	0.40	0.0018	1.74	2.93	1.008	24
0.126	0.986 ± 0.244	2.70	9.27	0.41	0.0062	1.70	2.74	1.043	30
0.168	0.586 ± 0.183	2.71	9.28	0.41	0.0061	1.71	2.75	1.027	24
0.225	0.517 ± 0.140	2.78	8.91	0.40	0.0063	1.77	3.09	1.073	25
0.273	0.572 ± 0.132	2.70	9.33	0.41	0.0082	1.69	2.69	1.083	33
0.329	0.422 ± 0.112	2.66	9.37	0.42	0.0080	1.67	2.61	1.051	27
0.371	0.416 ± 0.110	2.71	9.28	0.40	0.0099	1.71	2.74	1.093	29
0.418	0.227 ± 0.076	2.74	9.09	0.41	0.0072	1.74	2.93	1.087	18
0.485	0.271 ± 0.088	2.68	9.48	0.41	0.0098	1.67	2.56	1.107	18
0.531	0.255 ± 0.085	2.65	9.44	0.41	0.0082	1.66	2.54	1.107	17
0.559	0.140 ± 0.068	2.75	9.12	0.40	0.0081	1.74	2.90	1.116	8
0.625	0.182 ± 0.080	2.63	9.32	0.43	0.0111	1.66	2.63	1.114	10
0.668	0.167 ± 0.078	2.77	8.98	0.41	0.0096	1.77	3.04	1.110	8
0.717	0.072 ± 0.061	2.50	9.79	0.45	0.0098	1.55	2.08	1.126	3
0.776	0.128 ± 0.082	2.58	9.36	0.44	0.0101	1.63	2.51	1.123	5
0.806	0.029 ± 0.034	2.87	8.52	0.41	0.0034	1.86	3.53	1.152	1
0.875	0.266 ± 0.115	2.66	9.41	0.42	0.0103	1.67	2.57	1.197	8
0.926	0.121 ± 0.074	2.57	9.53	0.43	0.0090	1.61	2.39	1.224	4
1.017	0.129 ± 0.100	2.65	9.54	0.41	0.1048	1.66	2.50	1.339	2

Q^2 bins extended ±20% from the nominal Q^2 values listed in Table II. The constancy of W and Q^2 over the x' range achieved by these cuts can be seen in Tables III to VI.

VI. RESULTS

A. Structure-function x' dependence

Figures 5 through 9 show the invariant structure function as a function of x' for $p_T^2 < 0.02$ GeV^2. The displayed data are also tabulated in Tables III to VI. We restrict ourselves to the inclusive region, $x' < 0.7$, so as to exclude the πN and $\pi \Delta$ final states. The solid line in the figures is the result of a fit to the data discussed below and is given by

$$F(x') = 1.70 \exp(-3.25 x').\qquad(41)$$

The form of Eq. (41) is arbitrary and is not motivated by any physical model. The exponential factor is consistent with the parametrization of our earlier data,[18, 19] the SLAC results,[31] and the Fermilab muoproduction data.[32, 47] Even the hadron-induced reactions $\pi^\pm p \to \pi^\mp +$ anything are well described by the form of Eq. (41) for 8- and 16-GeV beam energies.[48]

For the hydrogen data, the π^+ at fixed W are strikingly constant over the entire Q^2 range. The π^- data, on the other hand, show an increasingly steep x' dependence as Q^2 increases. The dashed line in Figs. 5, 7, and 9 given by

$$F(x') = 1.43 \exp(-4.35 x')\qquad(42)$$

was determined from a fit to all the π^- data from hydrogen with $0 < x' < 0.7$ and $W \simeq 2.7$ GeV.

TABLE VI. The π^- structure function from deuterium and kinematic averages for $p_T^2 < 0.02$ GeV^2 as a function of x' (bin size is 0.05). The total cross section is for a proton target. Rad. corr. is an estimate of the radiative correction but is not applied to $F(x')$. N is the number of events in the bin.

x'	$F(x')$ (GeV^{-2})	W (GeV)	Q^2 (GeV^2)	ϵ	p_T^2 (GeV^2)	ω	σ_p (μb)	Rad. corr.	N
(a) $W = 2.2$ GeV, $Q^2 = 1.2$ GeV^2
0.049	0.899 ± 1.023	2.15	1.07	0.47	0.0014	4.48	46.50	1.002	1
0.077	0.906 ± 0.272	2.15	1.14	0.43	0.0006	4.33	44.10	1.018	31
0.126	1.046 ± 0.134	2.13	1.16	0.45	0.0007	4.23	44.20	1.055	117
0.175	0.916 ± 0.095	2.14	1.16	0.44	0.0013	4.23	43.70	1.040	184
0.223	0.828 ± 0.068	2.13	1.18	0.44	0.0018	4.16	43.44	1.088	273
0.277	0.590 ± 0.046	2.13	1.17	0.44	0.0020	4.18	43.58	1.100	286
0.325	0.500 ± 0.037	2.11	1.19	0.46	0.0031	4.06	43.44	1.068	290
0.374	0.396 ± 0.031	2.12	1.18	0.45	0.0045	4.13	43.49	1.112	296
0.427	0.303 ± 0.022	2.12	1.19	0.45	0.0053	4.10	43.45	1.106	316
0.475	0.299 ± 0.020	2.12	1.18	0.45	0.0065	4.12	43.70	1.127	360
0.525	0.233 ± 0.015	2.12	1.17	0.45	0.0064	4.15	43.75	1.127	353
0.575	0.201 ± 0.013	2.12	1.18	0.45	0.0075	4.14	43.57	1.137	348
0.624	0.207 ± 0.013	2.12	1.18	0.45	0.0072	4.14	43.72	1.134	381
0.674	0.163 ± 0.011	2.12	1.19	0.45	0.0069	4.10	43.47	1.129	357
0.726	0.167 ± 0.011	2.12	1.18	0.45	0.0074	4.10	43.62	1.145	373
0.777	0.193 ± 0.012	2.11	1.19	0.46	0.0080	4.05	43.57	1.141	420
0.825	0.239 ± 0.013	2.11	1.19	0.46	0.0078	4.08	43.57	1.169	538
0.872	0.183 ± 0.011	2.11	1.18	0.46	0.0082	4.07	43.69	1.212	411
0.923	0.087 ± 0.008	2.12	1.18	0.46	0.0081	4.11	43.88	1.235	202
0.984	0.312 ± 0.016	2.11	1.19	0.46	0.0082	4.03	43.51	1.343	673
1.010	0.206 ± 0.013	2.10	1.21	0.47	0.0081	3.96	43.30	1.343	434
1.067	0.008 ± 0.002	2.10	1.16	0.48	0.0080	4.08	44.42	1.343	15
(b) $W = 2.7$ GeV, $Q^2 = 2.0$ GeV^2
0.045	1.152 ± 0.692	2.57	2.13	0.37	0.0007	3.79	23.35	1.002	10
0.080	1.513 ± 0.227	2.67	1.92	0.33	0.0006	4.31	25.16	1.018	77
0.129	1.000 ± 0.118	2.68	1.96	0.32	0.0010	4.28	24.61	1.055	140
0.176	1.052 ± 0.086	2.67	1.95	0.33	0.0015	4.26	24.81	1.040	256
0.227	0.651 ± 0.057	2.67	1.93	0.33	0.0024	4.30	25.01	1.088	225
0.275	0.506 ± 0.039	2.67	1.94	0.33	0.0032	4.28	24.90	1.100	261
0.325	0.461 ± 0.033	2.67	1.95	0.33	0.0051	4.27	24.88	1.068	339
0.376	0.376 ± 0.024	2.67	1.95	0.33	0.0059	4.28	24.85	1.112	425
0.425	0.263 ± 0.018	2.67	1.94	0.34	0.0071	4.29	25.00	1.106	387
0.475	0.219 ± 0.015	2.66	1.96	0.34	0.0072	4.23	24.81	1.127	399
0.525	0.196 ± 0.013	2.66	1.96	0.34	0.0077	4.23	24.77	1.127	400
0.575	0.173 ± 0.011	2.66	1.97	0.34	0.0082	4.21	24.66	1.137	378
0.625	0.146 ± 0.010	2.66	1.96	0.34	0.0081	4.23	24.75	1.134	338
0.676	0.145 ± 0.010	2.66	1.95	0.34	0.0085	4.25	24.90	1.129	338
0.725	0.114 ± 0.009	2.66	1.95	0.34	0.0086	4.25	24.84	1.145	268
0.775	0.106 ± 0.008	2.66	1.95	0.34	0.0087	4.26	24.84	1.141	244
0.826	0.088 ± 0.008	2.65	1.99	0.34	0.0082	4.15	24.54	1.169	201
0.876	0.108 ± 0.009	2.66	1.94	0.34	0.0084	4.26	24.96	1.212	234
0.921	0.077 ± 0.007	2.66	1.95	0.34	0.0090	4.25	24.89	1.235	157
0.985	0.105 ± 0.009	2.64	2.01	0.35	0.0086	4.10	24.33	1.343	216
1.009	0.100 ± 0.010	2.65	1.98	0.35	0.0095	4.16	24.67	1.343	177
1.058	0.002 ± 0.002	2.63	2.05	0.35	0.0105	3.96	23.98	1.343	4
(c) $W = 2.7$ GeV, $Q^2 = 6.2$ GeV^2
0.038	1.255 ± 0.471	2.83	5.73	0.38	0.0013	2.24	6.93	1.002	20
0.074	0.828 ± 0.215	2.68	6.24	0.39	0.0012	2.02	5.72	1.018	40
0.130	0.709 ± 0.146	2.66	6.29	0.39	0.0029	2.00	5.62	1.055	66
0.173	0.782 ± 0.105	2.68	6.25	0.39	0.0054	2.03	5.76	1.040	115
0.224	0.547 ± 0.075	2.69	6.24	0.39	0.0062	2.03	5.77	1.088	108
0.272	0.269 ± 0.061	2.73	6.12	0.38	0.0079	2.09	6.04	1.100	62

TABLE VI. (Continued)

x'	$F(x')$ (GeV^{-2})	W (GeV)	Q^2 (GeV^2)	ϵ	p_T^2 (GeV^2)	ω	σ_p (μb)	Rad. corr.	N
0.327	0.278 ± 0.050	2.68	6.26	0.39	0.0075	2.02	5.72	1.068	74
0.377	0.312 ± 0.049	2.69	6.16	0.40	0.0077	2.04	5.88	1.112	98
0.425	0.266 ± 0.042	2.69	6.16	0.40	0.0086	2.05	5.92	1.106	96
0.473	0.188 ± 0.031	2.69	6.13	0.40	0.0091	2.05	5.96	1.127	76
0.524	0.168 ± 0.030	2.67	6.27	0.40	0.0103	2.02	5.72	1.127	68
0.566	0.084 ± 0.023	2.62	6.43	0.41	0.0105	1.95	5.35	1.137	32
0.620	0.114 ± 0.026	2.65	6.30	0.41	0.0094	2.00	5.60	1.134	42
0.671	0.100 ± 0.022	2.68	6.21	0.40	0.0104	2.03	5.84	1.129	39
0.727	0.073 ± 0.019	2.68	6.13	0.40	0.0107	2.04	5.92	1.145	26
0.773	0.093 ± 0.022	2.70	6.17	0.39	0.0093	2.06	5.96	1.141	30
0.822	0.054 ± 0.017	2.62	6.47	0.41	0.0019	1.94	5.27	1.169	15
0.874	0.068 ± 0.019	2.68	6.29	0.39	0.0074	2.02	5.70	1.212	19
0.921	0.042 ± 0.015	2.69	6.13	0.40	0.0094	2.06	6.00	1.235	11
0.982	0.030 ± 0.016	2.76	5.88	0.39	0.0131	2.15	6.52	1.343	7
1.008	0.035 ± 0.016	2.66	6.16	0.41	0.0125	2.02	5.82	1.343	8
1.077	0.007 ± 0.007	2.43	7.27	0.43	0.1028	1.69	3.74	1.343	1
(d) $W = 2.7$ GeV, $Q^2 = 9.5$ GeV^2									
0.012	0.566 ± 0.499	2.76	9.34	0.39	0.0017	1.72	2.73	1.002	4
0.074	1.175 ± 0.301	2.70	9.33	0.40	0.0033	1.70	2.72	1.018	24
0.127	0.564 ± 0.179	2.70	9.12	0.41	0.0036	1.71	2.82	1.055	21
0.176	0.700 ± 0.143	2.70	9.33	0.41	0.0061	1.70	2.72	1.040	37
0.220	0.566 ± 0.119	2.73	9.27	0.40	0.0076	1.71	2.77	1.088	37
0.277	0.253 ± 0.081	2.67	9.36	0.42	0.0093	1.68	2.65	1.100	23
0.317	0.385 ± 0.073	2.72	9.21	0.41	0.0087	1.71	2.79	1.068	46
0.371	0.297 ± 0.059	2.73	9.37	0.40	0.0082	1.70	2.70	1.112	42
0.426	0.194 ± 0.051	2.67	9.42	0.41	0.0099	1.67	2.58	1.106	30
0.477	0.203 ± 0.047	2.68	9.35	0.41	0.0108	1.68	2.64	1.127	29
0.531	0.102 ± 0.034	2.70	9.35	0.41	0.0110	1.69	2.68	1.127	15
0.570	0.121 ± 0.038	2.69	9.42	0.40	0.0096	1.68	2.62	1.137	16
0.622	0.072 ± 0.033	2.72	9.12	0.40	0.0072	1.73	2.88	1.134	8
0.674	0.084 ± 0.032	2.76	8.98	0.40	0.0094	1.76	3.01	1.129	10
0.721	0.088 ± 0.034	2.79	8.94	0.39	0.0081	1.78	3.08	1.145	10
0.783	0.030 ± 0.022	2.76	9.14	0.40	0.0140	1.74	2.89	1.141	3
0.840	0.016 ± 0.016	2.53	9.32	0.45	0.0114	1.60	2.38	1.169	1
0.885	0.030 ± 0.027	2.58	9.72	0.43	0.0065	1.61	2.33	1.212	2
0.922	0.018 ± 0.018	2.82	8.65	0.38	0.0085	1.82	3.32	1.235	1
1.016	0.031 ± 0.032	2.50	9.99	0.44	0.0033	1.54	1.97	1.343	1

For the deuterium data the π^+ data again show a Q^2 independence of the x' dependence except for $Q^2 = 9.3$ GeV^2, where the data are slightly lower. The π^- data show the same steepening of the x' dependence with increasing Q^2 as the hydrogen data.

In order to study the behavior more closely in the region $0 < x' < 0.7$, the structure functions have been fit to the form

$$F(x') = A\exp(-Bx') . \qquad (43)$$

The results are shown in Table VII. Included for the purposes of this fit only are data at $W = 3.1$ GeV and $Q^2 = 4.5$ GeV^2, which were extracted from the (W, Q^2) region of another point excluded by the (W, Q^2) binning cuts. These data were used to ex-

tend the fits at $W = 3.1$ GeV to larger values of $1/\omega$. Figure 10 summarizes the results of this fit for hydrogen as a function of ω for this experiment and the earlier Harvard data. For the π^+ data, the A and B coefficients are remarkably independent of Q^2 and ω. Thus the π^+ invariant structure function displays trivial Bjorken scaling and the x' dependence is not a function of Q^2. This is Feynman scaling and indicates that the π^+ invariant cross section scales in ω in the same manner as the total virtual photoproduction cross section. On the other hand, the π^- structure function changes with ω and is consistent with becoming a universal, nontrivial function of ω as W increases. The A and B parameters for the 2.7-GeV and 3.1-GeV data lie on the same curve indi-
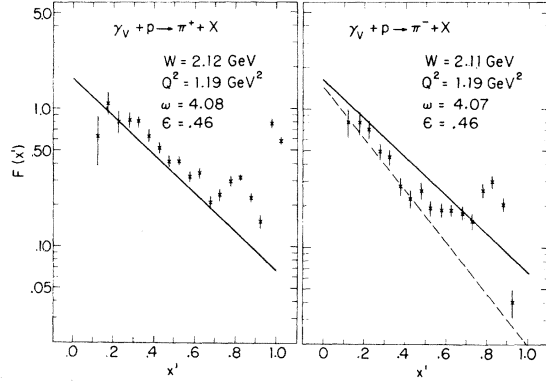
FIG. 5. Pion structure functions for a hydrogen target for $p_T^2 < 0.02$ GeV^2 and $W \sim 2.2$ GeV. The solid lines are given by $F(x') = 1.70 \exp(-3.25x')$; the dashed line is given by $1.43 \exp(-4.35x')$.

cating no W dependence for $W \gtrsim 2.6$ GeV. Thus the π^- structure function appears to display Bjorken scaling at the higher values of W.

For $W > 2.6$ GeV, we have fit the parameter A of Fig. 10 to a constant with the results

$$A(\pi^+, p) = 1.70 \pm 0.04 \quad (\chi^2/\text{DOF} = 5.5/9),$$

$$A(\pi^-, p) = 1.42 \pm 0.03 \quad (\chi^2/\text{DOF} = 2.0/7) \tag{44}$$

(DOF is degrees of freedom). We fit the param-

FIG. 7. Structure functions for π^- production from hydrogen for $p_T^2 < 0.02$ GeV^2. The solid lines are given by $F(x') = 1.70 \exp(-3.25x')$ and are a fit to the π^+ data; the dashed lines are given by $F(x') = 1.43 \exp(-4.35x')$ and are a fit to the π^- data.
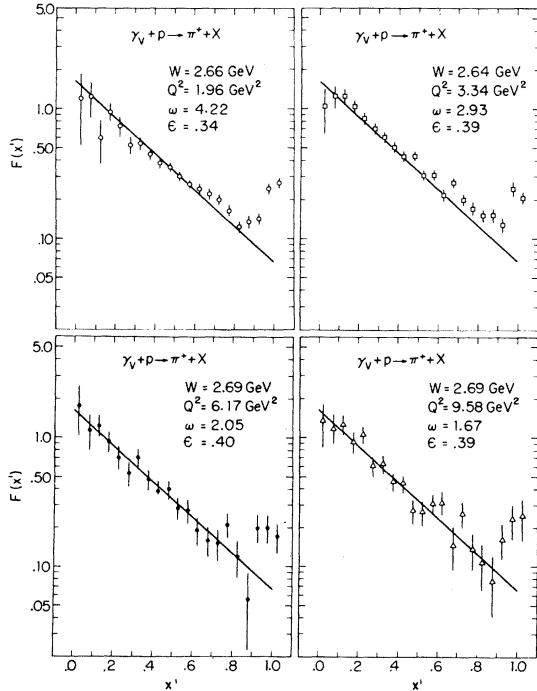
FIG. 6. Structure functions for π^+ production from hydrogen for $p_T^2 < 0.02$ GeV^2 and $W \sim 2.7$ GeV. The solid lines are given by $F(x') = 1.70 \exp(-3.25x')$.
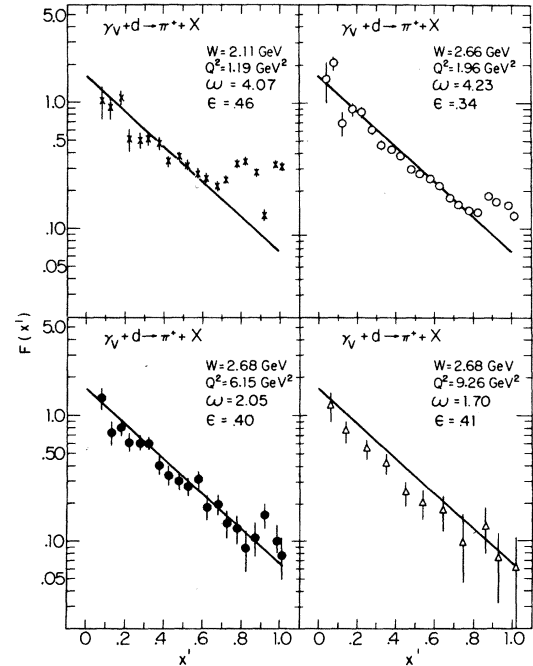
FIG. 8. Structure functions for π^+ production from deuterium for $p_T^2 < 0.02$ GeV^2. The solid lines are given by $F(x') = 1.70 \exp(-3.25x')$ and are a fit to the π^+ data obtained with a hydrogen target.
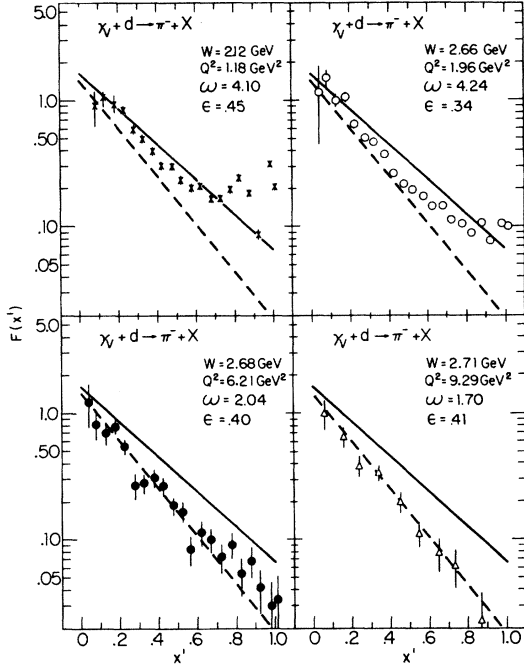
FIG. 9. Structure functions for π^- production from deuterium for $p_T^2 < 0.02$ GeV^2. The solid lines are given by $F(x') = 1.70\exp(-3.25x')$ and are a fit to the π^+ data obtained with a hydrogen target. The dashed lines are given by $F(x') = 1.43\exp(-4.35x')$ and are a fit to the π^- data obtained with a hydrogen target.

eter B to a constant and also to a constant plus a $1/\omega$ term with the results

$$B(\pi^+, p) = \begin{cases} 3.25 \pm 0.06 \quad (\chi^2/\text{DOF} = 8.9/9) \\ (3.30 \pm 0.13) - (0.19 \pm 0.47)1/\omega \qquad (45) \\ (\chi^2/\text{DOF} = 8.8/8), \end{cases}$$

$$B(\pi^-, p) = \begin{cases} 4.08 \pm 0.15 \quad (\chi^2/\text{DOF} = 15.9/7) \\ (3.36 \pm 0.05) + (2.89 \pm 0.17)1/\omega \qquad (46) \\ (\chi^2/\text{DOF} = 0.3/6). \end{cases}$$

On the basis of χ^2, $B(\pi^+, p)$ is consistent with being a constant and $B(\pi^-, p)$ requires the additional $1/\omega$ dependence.

Figure 11 summarizes the results of the fits to Eq. (43) for the deuterium data. For $W > 2.6$ GeV the π^+ data are again nearly independent of ω. The π^- again exhibit a steepening x' dependence with increasing $1/\omega$. To demonstrate this we proceed as with the hydrogen data and fit the parameter A to a constant,

$$A(\pi^+, d) = 1.48 \pm 0.10 \quad (\chi^2/\text{DOF} = 10.4/4),$$
$$A(\pi^-, d) = 1.47 \pm 0.12 \quad (\chi^2/\text{DOF} = 10.2/4). \qquad (47)$$

Fits for the parameter B as a function of ω yielded

$$B(\pi^+, d) = \begin{cases} 3.08 \pm 0.09 \quad (\chi^2/\text{DOF} = 2.9/4) \\ (3.06 \pm 0.19) + (0.08 \pm 0.59)/\omega \qquad (48) \\ (\chi^2/\text{DOF} = 2.9/3), \end{cases}$$

$$B(\pi^-, d) = \begin{cases} 3.78 \pm 0.16 \quad (\chi^2/\text{DOF} = 6.4/4) \\ (3.32 \pm 0.20) + (1.68 \pm 0.62)/\omega \qquad (49) \\ (\chi^2/\text{DOF} = 1.9/3). \end{cases}$$

The parameter A for π^+ and π^- are consistent with being equal and also equal to $A(\pi^-, p)$. For large ω, this indicates nearly equal production of π^- from protons and neutrons and less π^+ production from neutrons relative to protons. $B(\pi^-, d)$ appears to require the $1/\omega$ term while $B(\pi^+, d)$ does not as in the hydrogen results. The $1/\omega$ dependence of $B(\pi^-, d)$ is weaker, indicating that the x' slope parameter for π^- production from neutrons has a weaker $1/\omega$ dependence than $B(\pi^-, p)$ and may even be independent of ω. Interestingly, for $\omega \gg 1$ all four B's are nearly equal. In other words, for large ω, all the structure functions approach a limiting shape as a function of x'.

To test the limiting-fragmentation hypothesis we have formed the ratio of the deuteron to proton structure functions. If limiting fragmentation is applicable in our W, Q^2 region we would expect this ratio to be unity in the photon fragmentation region, $x' > 0$. In Fig. 12 we see that this is only approximately true in the inclusive region. In Table VIII we show the average ratio for $0.2 < x' < 0.7$. For π^+, the ratio is consistently less than one, indicating a lower production of π^+'s from neutrons than from protons. For π^-, the ratio is consistently greater than unity indicating that π^- production from neutrons is greater than from protons. The derived ratio of neutron to proton structure functions is also shown in the table. Limiting fragmentation does not appear to be true at our values of W. This may be due to the absence of a central plateau in rapidity to separate completely the target and photon regions. The DESY π^- data indicate that the target fragmentation region is independent of Q^2 at energies comparable to ours.[26]

If the contribution due to sea quarks is neglected, Eq. (25) and its analog for a neutron target can be used to establish the size of $\eta(x') = D_u^+(x')/D_u^-(x')$ relative to one. A ratio of the π^+ structure functions for neutrons and protons less than one and a ratio of the π^- greater than one both imply $\eta(x') > 1$. A more direct and quantiative extraction of $\eta(x')$ will be made below.

TABLE VII. Results of fitting pion structure functions to $Ae^{-Bx'}$ for $0.0 < x' < 0.7$ and $p_T^2 < 0.02$ GeV^2.

W (GeV)	Q^2 (GeV^2)	$1/\omega$	A (GeV^{-2})	B	χ^2/DOF
(a) π^+ from protons
2.2	1.2	0.25	1.66 ± 0.24	2.79 ± 0.29	21/11
2.2[a]	1.2	0.24	1.80 ± 0.16	3.03 ± 0.22	16/11
2.2[a]	2.0	0.35	1.89 ± 0.18	3.18 ± 0.21	15/12
2.2[a]	4.0	0.52	1.73 ± 0.24	3.07 ± 0.31	12/12
2.7[b,c]	1.2	0.15	1.71 ± 0.28	3.08 ± 0.30	20/8
2.7	2.0	0.24	1.49 ± 0.13	2.92 ± 0.17	12/12
2.7[a]	2.0	0.24	1.78 ± 0.11	3.32 ± 0.14	10/11
2.7	3.3	0.34	1.62 ± 0.13	2.98 ± 0.17	16/12
2.7	3.3	0.35	1.79 ± 0.16	3.32 ± 0.20	8/12
2.7	6.2	0.49	1.69 ± 0.15	3.33 ± 0.22	6/12
2.7	9.5	0.60	1.74 ± 0.20	3.40 ± 0.30	11/12
3.1[a]	1.2	0.12	1.74 ± 0.10	3.33 ± 0.13	17/12
3.1[a]	1.7	0.16	1.76 ± 0.09	3.37 ± 0.11	8/12
3.1[c]	4.5	0.33	1.40 ± 0.30	3.19 ± 0.54	5/8
(b) π^- from protons
2.2	1.2	0.25	1.04 ± 0.19	2.95 ± 0.37	19/10
2.2[a]	1.2	0.24	1.14 ± 0.13	3.22 ± 0.28	26/12
2.2[a]	4.0	0.52	1.50 ± 0.22	4.08 ± 0.39	8/12
2.7	2.0	0.24	1.43 ± 0.14	4.13 ± 0.24	16/11
2.7[b]	2.0	0.24	1.31 ± 0.33	4.01 ± 0.58	28/12
2.7	3.3	0.34	1.45 ± 0.14	4.37 ± 0.25	17/12
2.7	6.2	0.49	1.53 ± 0.18	4.66 ± 0.34	10/12
2.7	9.5	0.60	1.27 ± 0.19	5.10 ± 0.46	6/11
3.1[a]	1.2	0.12	1.37 ± 0.10	3.68 ± 0.18	11/11
3.1[a]	1.7	0.16	1.45 ± 0.14	3.77 ± 0.27	18/12
3.1	4.5	0.33	1.56 ± 0.19	4.42 ± 0.52	9/10
(c) π^+ from deuterons
2.2	1.2	0.25	1.31 ± 0.15	2.43 ± 0.22	14/11
2.2[a]	1.2	0.24	1.15 ± 0.15	2.45 ± 0.30	42/11
2.2[a]	4.0	0.52	2.11 ± 0.20	3.82 ± 0.24	10/12
2.7	2.0	0.24	1.70 ± 0.18	3.18 ± 0.22	26/12
2.7	6.2	0.49	1.46 ± 0.13	2.82 ± 0.23	9/12
2.7	9.5	0.60	1.52 ± 0.18	3.47 ± 0.35	5/12
3.1[a]	1.2	0.12	1.31 ± 0.09	3.04 ± 0.16	26/12
3.1	4.5	0.33	1.87 ± 0.17	3.18 ± 0.30	10/12
(d) π^- from deuterons
2.2	1.2	0.25	1.74 ± 0.15	3.41 ± 0.19	19/11
2.2[a]	1.2	0.24	1.15 ± 0.10	3.00 ± 0.20	23/11
2.2[a]	4.0	0.52	1.87 ± 0.22	4.56 ± 0.32	13/11
2.7	2.0	0.24	1.84 ± 0.19	3.90 ± 0.23	33/12
2.7	6.2	0.49	1.42 ± 0.20	4.04 ± 0.36	16/12
2.7	9.5	0.60	1.41 ± 0.21	4.16 ± 0.40	10/12
3.1[a]	1.2	0.12	1.23 ± 0.12	3.37 ± 0.21	35/12
3.1	4.5	0.33	1.74 ± 0.18	4.15 ± 0.39	12/11

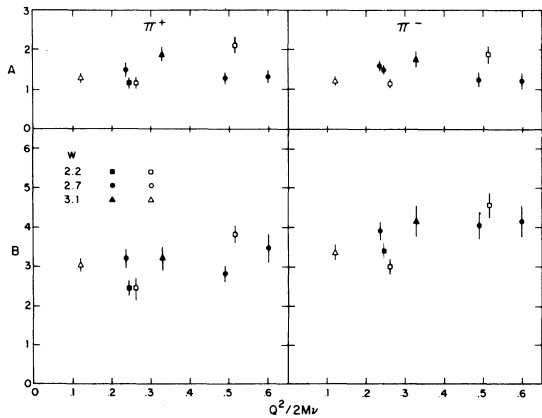[a]Reference 19.　　　　　　[b]Reference 18.　　　　　　[c]$0.2 \leqslant x' \leqslant 0.7$.
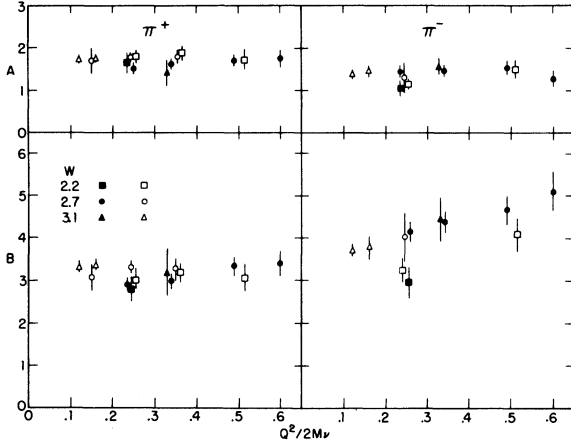
FIG. 10. Results of fits to $Ae^{-Bx'}$ for the pion structure functions from hydrogen. The solid points are from the present experiment and the open points are from fits to the data in Refs. 18 and 19.

B. Structure-function p_T dependence

The structure function is usually assumed to be factorable into an x' and a p_T dependence:

$$F(x', p_T) \rightarrow F(x')h(p_T^2). \tag{50}$$

A common parametrization of $h(p_T^2)$ is a simple exponential

$$h(p_T^2) \propto \exp(-bp_T^2), \tag{51}$$

even though deviation from this form is seen at large p_T.[47,49] The limited p_T acceptance of our apparatus and the smallness of b make a determination of b difficult with these data. The proton

FIG. 11. Results of fits to $Ae^{-Bx'}$ for the pion structure functions from deuterium. The solid points are from the present experiment and the open points are from fits to the data of Ref. 19.
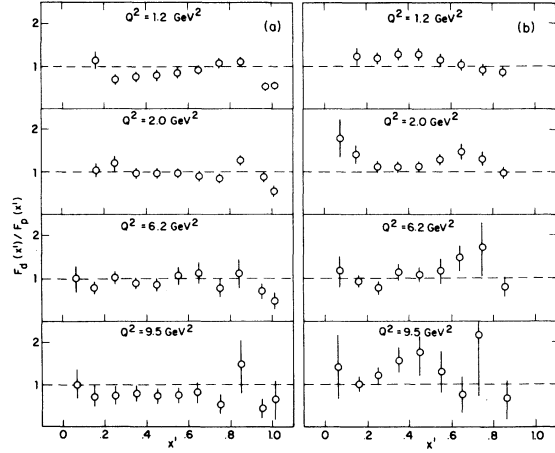
FIG. 12. The ratio of structure functions from hydrogen and deuterium as a function of x' for (a) π^+ and (b) π^-.

and deuteron data for π^+ have been fitted for b in three x' regions and the results are shown as a function of Q^2 in Fig. 13. The parameter is consistent with a value of ~ 4 GeV^{-2} at all Q^2 and x'.

Results exist from other experiments that give a better measurement of b or $\langle p_T^2 \rangle$. The results divide into two Q^2 regions. For $Q^2 \lesssim 1$ GeV^2, $\langle p_T^2 \rangle$ increases from $Q^2 = 0$ to $Q^2 \sim 0.5$ GeV^2, where $\langle p_T^2 \rangle$ begins to flatten out.[26] For $Q^2 \gtrsim 1$ GeV^2, $\langle p_T^2 \rangle$ is found to be independent of Q^2 out to 25 GeV^2 (see Ref. 29). The latter experiment observed events over the entire p_T range. Vector-meson-dominance electroproduction models suggest such an increase in $\langle p_T^2 \rangle$ as Q^2 increases to $Q^2 \sim M_\rho^2 \sim 0.5$ GeV^2, where the ρ nature of the photon becomes dominated by the bare pointlike photon.

Recent muoproduction results[47] indicate that Eq. (50) is not a valid separation of the x' and p_T dependencies of the structure function. As a function of x', $\langle p_T \rangle$ increases from ~ 350 MeV at x' ~ 0 to a maximum of ~ 500 MeV at $x' \sim 0.5$ and then decreases to ~ 350 MeV at $x' \sim 1$. This effect shows that the p_T dependence of F cannot be simply parametrized by Eqs. (50) and (51).

C. Charge ratios

The ratio of the number of π^+ to π^- is a sensitive test of the differences in π^+ and π^- electroproduction and of the predictions of certain theoretical models. The small- and large-p_T dependencies of the ratio were extensively studied in earlier Harvard-Cornell experiments.[19,49] No dependence was found.

Figure 14 shows the π^+/π^- ratio as a function of x' for this experiment and the earlier Harvard ex-

TABLE VIII. The ratio of pion structure functions from protons and deuterons for $0.2 < x'$ < 0.7 and $p_T^2 < 0.02$ GeV^2 and the implied ratio from protons and neutrons.

W (GeV)	Q^2 (GeV^2)	ω	$\langle F_d/F_p \rangle_{\pi^+}$	$\langle F_n/F_p \rangle_{\pi^+}$	$\langle F_d/F_p \rangle_{\pi^-}$	$\langle F_n/F_p \rangle_{\pi^-}$
2.2	1.2	4.1	0.76 ± 0.03	0.47 ± 0.07	1.12 ± 0.05	1.27 ± 0.11
2.7	2.0	4.2	0.87 ± 0.03	0.71 ± 0.07	1.15 ± 0.05	1.33 ± 0.11
2.7	6.2	2.1	0.91 ± 0.07	0.77 ± 0.18	0.85 ± 0.08	0.62 ± 0.20
2.7	9.5	1.7	0.64 ± 0.08	0.00 ± 0.22	1.11 ± 0.17	1.31 ± 0.47

periments. For $W < 2.8$ GeV the ratio is a function of x', increasing as x' increases. At large values of x' the ratio decreases because the cross section for the $\pi^- \Delta^{++}$ channel is larger than that for the $\pi^+ \Delta^0$ channel. At the highest W the ratio is independent of x'. In the Dakin-Feldman quark model $\eta(x')$, the ratio of the u-quark fragmentation probabilities into π^+ and π^-, is assumed to be independent of x'. The π^+/π^- ratio should also be independent of x'. This does not appear to be true for $W \lesssim 2.7$ GeV.

The fits of the structure-function x' dependence predict a residual x' dependence of the charge ratio which decreases with increasing ω. From Eqs. (44), (45), and (46), the charge ratio from protons is predicted to be

$$\frac{\langle n_{\pi^+} \rangle}{\langle n_{\pi^-} \rangle} \simeq 1.20 \exp(-2.89 x'/\omega). \tag{52}$$

Interestingly, photoproduction ($1/\omega = 0$) results for the charge ratio also find a value of 1.20 (see Ref. 50).

We have examined the charge ratio for events produced in the region $0.3 < x' < 0.7$ defined as

$$\frac{\langle n_{\pi^+} \rangle}{\langle n_{\pi^-} \rangle} = \frac{\int_{0.3}^{0.7} \frac{\sigma_{tot}}{E^*} F^+(x') dx'}{\int_{0.3}^{0.7} \frac{\sigma_{tot}}{E^*} F^-(x') dx'}, \tag{53}$$

where $F(x')$ is the p_T- and ϕ-averaged structure functions in Figs. 5 through 9. In addition to the new data, the data from the earlier Harvard-Cornell and Harvard experiments were reanalyzed according to Eq. (53). The results are given in Table IX and are displayed in Fig. 15 plotted versus $1/\omega$, the natural scaling variable of parton models, and versus W, the natural scaling variable of thermodynamic models. In the past it has been difficult to distinguish between a $1/\omega$ and a W dependence. With the present data included, the charge ratio seems to favor a universal $1/\omega$ dependence. The curves in the figure are the Dakin and Feldman theory with $\eta = 2.2 \pm 0.1$ determined from a fit to the hydrogen data in the figure.

The parton-theory prediction that the single variable $1/\omega$ parametrizes the charge ratio is a good description of the data. Thermodynamic models predict the ratio to approach unity with increasing W due to the increasing multiplicity of particles diluting any initial charge of the target nucleon.
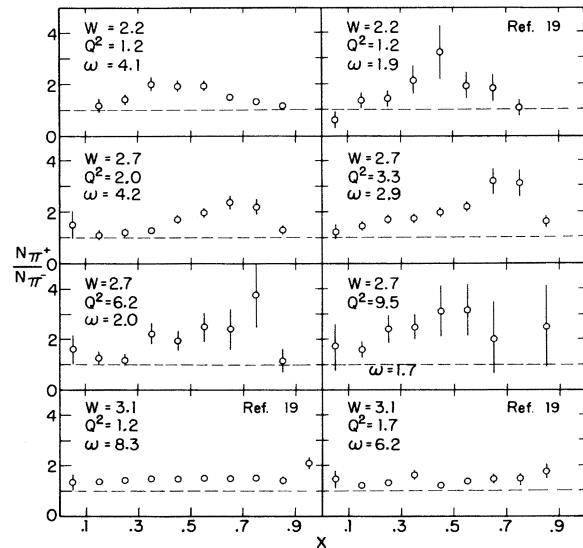

FIG. 13. The results of a fit to the combined hydrogen and deuterium structure functions for π^+ of the form $ae^{-b p_T^2}$ for $p_T^2 < 0.20$ GeV^2. The parameter b is shown as a function of Q^2 for (a) $0.3 < x' < 0.5$, (b) $0.5 < x' < 0.7$, (c) $0.7 < x' < 0.9$.

FIG. 14. The charged-pion ratio (π^+/π^-) as a function of x' for several values of W and Q^2.

TABLE IX. Pion charge ratio for $p_T^2 < 0.02$ GeV^2.

W (GeV)	Q^2 (GeV^2)	$1/\omega$	$0.1 < x' < 0.3$	π^+/π^- $0.3 < x' < 0.7$	$0.7 < x' < 0.9$
			(a) Protons		
2.2	1.2	0.24	1.90 ± 0.18	1.90 ± 0.12	1.21 ± 0.08
2.2[a]	1.2	0.24	1.61 ± 0.12	1.71 ± 0.10	0.92 ± 0.07
2.2[a]	2.0	0.33	$\cdots$	2.42 ± 0.35	1.34 ± 0.17
2.2[a]	4.0	0.50	1.54 ± 0.28	1.99 ± 0.31	1.70 ± 0.37
2.7	2.0	0.24	1.36 ± 0.14	1.71 ± 0.08	1.74 ± 0.15
2.7[b]	2.0	0.23	1.13 ± 0.13	1.82 ± 0.17	1.57 ± 0.17
2.7	3.3	0.33	1.52 ± 0.12	1.97 ± 0.11	2.22 ± 0.23
2.7[a]	3.3	0.33	$\cdots$	$\cdots$	1.90 ± 0.45
2.7	6.2	0.49	1.25 ± 0.16	2.20 ± 0.25	2.14 ± 0.55
2.7	9.5	0.60	1.91 ± 0.28	2.39 ± 0.43	5.41 ± 2.38
3.1[a]	1.2	0.12	1.34 ± 0.08	1.47 ± 0.08	1.43 ± 0.10
3.1[a]	1.7	0.16	1.22 ± 0.09	1.45 ± 0.09	1.60 ± 0.18
			(b) Deuterons		
2.2	1.2	0.24	0.89 ± 0.09	1.21 ± 0.06	1.53 ± 0.06
2.2[a]	1.2	0.23	1.20 ± 0.08	1.28 ± 0.06	1.35 ± 0.06
2.2[a]	4.0	0.50	1.25 ± 0.13	1.47 ± 0.13	1.76 ± 0.28
2.7	2.0	0.24	0.94 ± 0.08	1.24 ± 0.05	1.45 ± 0.08
2.7	6.2	0.49	1.25 ± 0.16	1.78 ± 0.16	1.59 ± 0.31
2.7	9.5	0.60	1.31 ± 0.25	1.37 ± 0.21	2.46 ± 1.09
3.1[a]	1.2	0.12	1.09 ± 0.05	1.30 ± 0.05	1.17 ± 0.16
			(c) Neutrons		
2.2	1.2	0.24	0.67 ± 0.20	0.61 ± 0.11	2.10 ± 0.29
2.2[a]	1.2	0.23	0.78 ± 0.17	0.84 ± 0.12	2.01 ± 0.25
2.2[a]	4.0	0.50	1.07 ± 0.35	0.65 ± 0.32	2.04 ± 1.09
2.7	2.0	0.24	0.64 ± 0.16	0.84 ± 0.10	1.19 ± 0.18
2.7	6.2	0.49	1.05 ± 0.67	1.21 ± 0.36	0.91 ± 0.69
2.7	9.5	0.60	0.23 ± 0.52	0.32 ± 0.34	1.02 ± 1.73
3.1[a]	1.2	0.12	0.83 ± 0.12	1.11 ± 0.12	0.91 ± 0.12

[a]Reference 19.   [b]Reference 18.
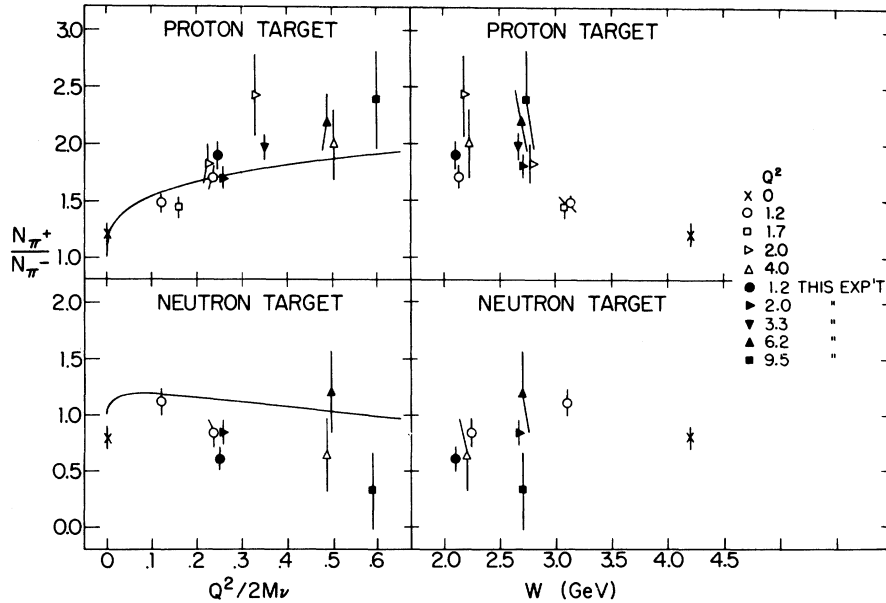
FIG. 15. The charged-pion ratio for proton and neutron targets as a function of the scaling variables $1/\omega$ and W. The photoproduction results are from Ref. 50 and the open points are from Refs. 18 and 19. The curves are the result of a fit to a simple quark model.
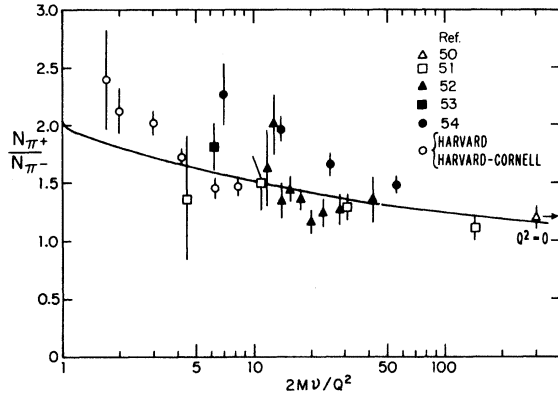
FIG. 16. The pion charge ratio for hydrogen from several experiments as a function of ω. The curve is the result of a fit to a simple quark model.

The data do appear to approach one as W increases, but this single variable is not sufficient to describe the data completely. Vector-meson dominance predicts a ratio of 1 if the vector-meson–nucleon interaction is diffractive since the photon is neutral. The limiting-fragmentation picture also predicts a charge ratio of one in the photon fragmentation region, $x' > 0$, again because the photon is neutral. The initial proton charge should appear in the region $x' < 0$. In Fig. 16, we summarize the present world data for the pion charge ratio from hydrogen as a function of ω.[18,19,50-54] Again the curve is the Dakin and Feldman theory with $\eta = 2.2$. All the data except for the recent SLAC results[54] are in good agreement. The reason the SLAC results disagree may be the x' region over which the ratio is calculated, $0.4 < x < 0.85$. If the charge ratio is a function of x', as has been seen for small ω and W, the SLAC ratios would tend to be larger due to the larger x' values used in the calculation relative to the other experiments in this kinematic region.

D. Factorizability of the distribution and fragmentation functions

In many parton models it is assumed that the parton distribution and fragmentation functions are independent functions of x_B and x, respectively, and that it is their products that contribute to the structure function. Feynman has pointed out that this assumption could be tested by taking the difference of the π^+ and π^- structure functions. From the quark-parton ideas discussed above we can write

$$\frac{1}{\sigma_{tot}} \frac{d\sigma}{dx} = \frac{\sum_{i=1}^{6} e_i^2 q_i(x_B) D_i(x)}{\sum_{i=1}^{6} e_i^2 q_i(x_B)} , \tag{54}$$
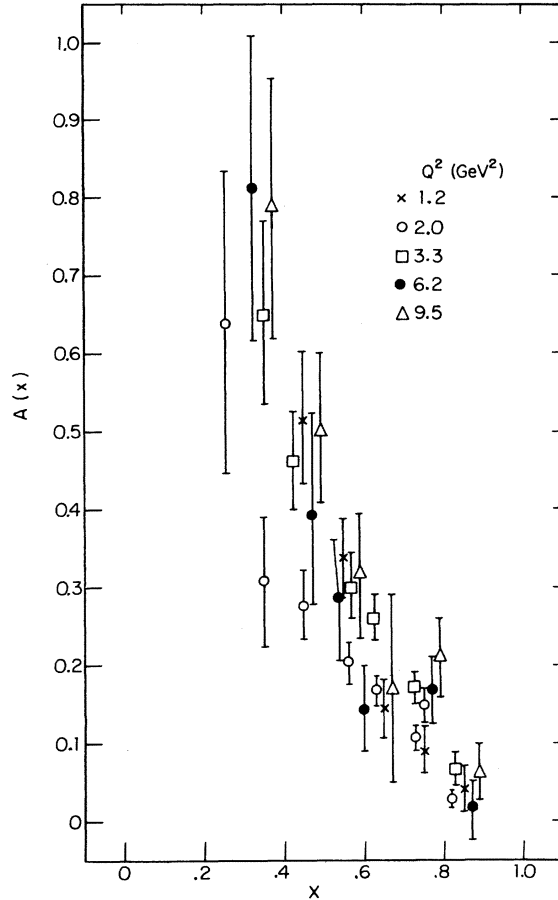
FIG. 17. The difference of $u(d)$ quark fragmentation probabilities into π^+ (π^-) and π^- (π^+) as a function of x for several values of Q^2.

where q_i and e_i are the six quarks' distribution functions and charges. For our purposes here we neglect the difference between x and x'. In terms of the measured structure function.

$$\frac{1}{\sigma_{tot}} \frac{d\sigma}{dx} = \frac{\pi}{b} \frac{p_{max}^*}{E^*} F(x) . \tag{55}$$

The factorization of the structure function's x and p_T dependencies has been assumed and an average over ϕ performed. The factor b is the p_T^2 exponential parameter of Eq. (51). From the two equations we have

$$\frac{\pi}{b} \frac{p_{max}^*}{E^*} [F^+(x) - F^-(x)]$$

$$= [D_u^+(x) - D_u^-(x)] \left[\frac{4u_v(x_B) - d_v(x_B)}{4u_v(x_B) + d_v(x_B) + 12c(x_B)} \right]$$

$$= A(x)G(x_B) . \tag{56}$$

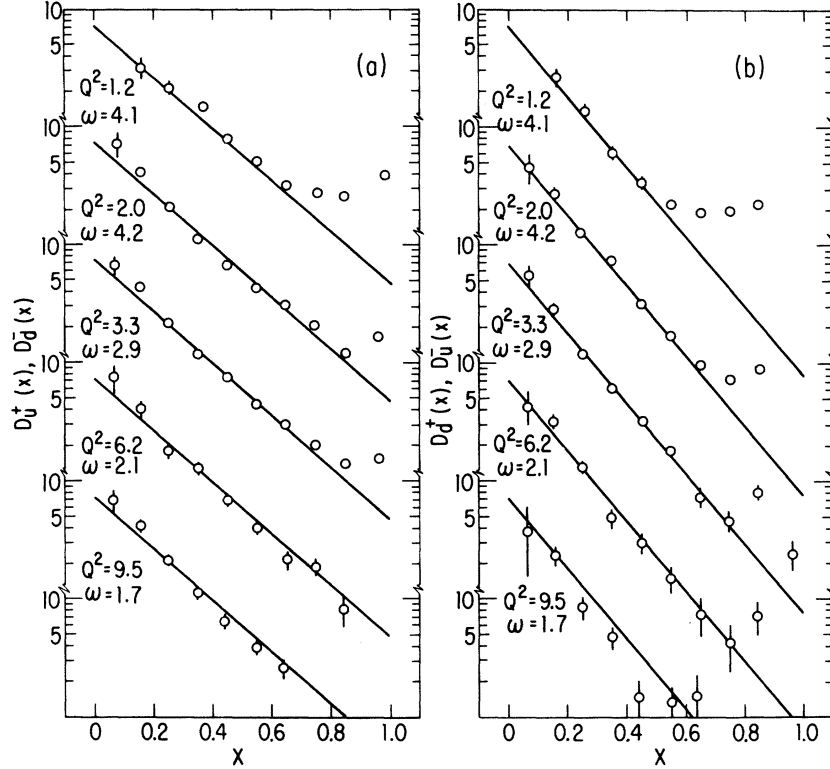The factorization into an x and an x_B term is quite general. If it can be shown that $A(x)$ is a universal

FIG. 18. The fragmentation probabilities of (a) u quarks into π^+ or d quarks into π^- and (b) u quarks into π^- or d quarks into π^+ as a function of x for several values of ω. The solid line in part (a) is given by $7.38\exp(-5.05x)$ and was obtained from a fit to the four highest Q^2 points for $0<x<0.7$. The solid line in part (b) is given by $7.20\exp(-6.85x)$ and was obtained from a fit to the four highest Q^2 points for $0<x<0.7$.

function of x, the factorization of the distribution and fragmentations functions can be verified.

In Fig. 17 we show the extracted function $A(x)$ for our hydrogen data. $G(x_B)$ was calculated from the distribution function fits of Eq. (23). The b parameter was assumed to be independent of W, Q^2, and pion charge, and equal to 4 GeV^{-2}. $A(x)$ is consistent with a universal function of x. A comment on $G(x_B)$: it varies by only 20% over the Q^2 range so that the extent to which the product of G and A remains constant at fixed x is not severely tested, but the result is interesting.

Assuming the factorization of distribution and fragmentation functions seen above and neglecting the contributions of the sea quarks, we have extracted the fragmentation functions of the u and d quarks into pions. Defining

$$H^+ = \frac{\pi}{b}\frac{p_{max}^*}{E^*}F^+(x)f_{ep}(x_B) , \tag{57}$$

and defining H^- analogously we can write

$$D_u^+(x) = D_d^-(x) = \frac{9[4u_v(x_B)H^+ - d_v(x_B)H^-]}{16u_v^2(x_B) - d_v^2(x_B)} , \tag{58a}$$

$$D_u^-(x) = D_d^+(x) = \frac{9[4u_v(x_B)H^- - d_v(x_B)H^+]}{16u_v^2(x_B) - d_v^2(x_B)} . \tag{58b}$$

In Fig. 18 are shown the derived fragmentation functions for the hydrogen data. The line in Fig. 18(a) is the result of a fit to the four highest Q^2 points for $0<x<0.7$, which gave

$$D_u^+(x) = 7.38\exp(-5.05x) . \tag{59}$$

The line in Fig. 18(b) is the result of a similar fit, which gave

$$D_u^-(x) = 7.20\exp(-6.85x) . \tag{60}$$

The lines are intended only as a guide for comparing the data. Away from the resonance region, $x<0.7$, the fragmentation functions exhibit no ω dependence. This is to be contrasted with the structure functions, in particular those for π^-, which exhibit an ω dependence. Figure 18 shows that the ω dependence of the structure functions arises only from the quark distribution functions as the quark-parton model requires.

The inclusive production of hadrons by neutrinos separately measures $D_u^+(x)$ and $D_u^-(x)$. The steeper x dependence for $D_u^-(x)$ relative to $D_u^+(x)$ is observed
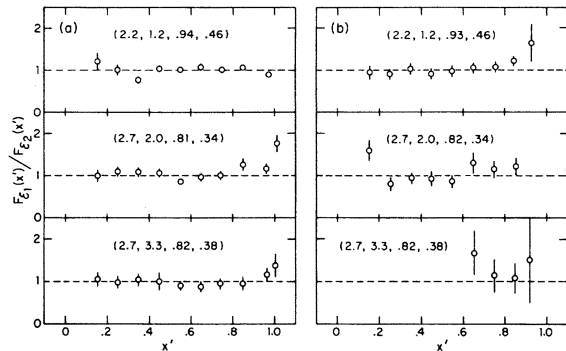
FIG. 19. The ratio of the structure functions for protons for two ϵ values at several $(W, Q^2, \epsilon_1, \epsilon_2)$ points for (a) π^+ and (b) π^-.

in a neutrino experiment which measures the structure function for charged hadrons.[55]

The ratio of $D_u^+(x)$ to $D_u^-(x)$, $\eta(x)$, in the charge ratio is not independent of x as can be seen from Eqs. (59) and (60). This was the conclusion from the above discussion of the x dependence of the charge ratio.

E. Scalar-transverse separation

A unique feature of the data from this experiment is the low value of the photon polarization parameter. Using data from the earlier Harvard-Cornell[18] and Harvard[19] experiments (data points 6, 7, 8, and 11), where ϵ was approximately 0.9, and the present data, where ϵ is approximately 0.4, a separation of the pion inclusive structure function can be made at three (W, Q^2) points. Data points 6 and 8 from the earlier experiments were at the same (W, Q^2, ϵ) points and the results have been combined.

In Figs. 19 and 20 we display the ratio of pion structure functions for fixed (W, Q^2) and different values of ϵ. The ratios are nearly one, indicating that the pion inclusives are consistent with the same scalar-photon component as the total cross section. In Fig. 21 we show the missing-mass spectrum for two values of ϵ with (W, Q^2) fixed. The $\epsilon = 0.94$ is from the earlier Harvard experiment.[56] The $\pi^+ n$ channel is a strong function of ϵ while the $\pi^+ \Delta^0$ and the inclusion region are nearly the same for the two ϵ values.

In Table X we show the ratio of the invariant cross section $E d^3\sigma/dp^3$ for $p_T^2 < 0.02$ GeV^2 for several x' regions. If we write for this cross section

$$E \frac{d^3\sigma}{dp^3} = A + \epsilon C , \tag{61}$$

the results in Table X are

$$\frac{A + \epsilon_1 C}{A + \epsilon_2 C} . \tag{62}$$

In Table XI we show the scalar-transverse ratio, $R = C/A$, calculated from Table X. R is found to be consistent with zero and with the value found from deep-inelastic scattering, 0.14 ± 0.07 (see Ref. 57). In the context of the parton model this implies spin-$\frac{1}{2}$ constituents for the nucleon.

The spectrometers used in the earlier high-ϵ experiments were also checked with elastic scattering measurements. The mean ratios of the measured cross sections to the average of the world data for the electron and hadron arms were 0.994 ± 0.007 and 0.998 ± 0.009, respectively. The estimated systematic uncertainty in the high-ϵ data is $\pm 7\%$. The same Faraday cup was used in all experiments. Since the two spectrometer systems and the procedure of data analysis were very similar, we believe the systematic uncertainties to be correlated such that the systematic uncertainty in Table X is $\pm 10\%$, one third of which is due to the uncorrelated portion. This uncorrelated portion introduces an uncertainty in R of ± 0.06. The results in Table XI do not include this systematic uncertainty.

F. Forward multiplicities

An interesting exercise is the calculation of the particle multiplicity in the forward hemisphere

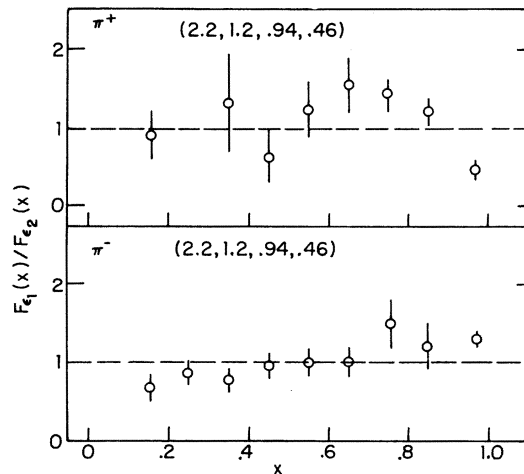$$\langle n \rangle = \frac{1}{\sigma_T} \int_{x'>0} \frac{d^3\sigma}{dp^3} dp^3 . \tag{63}$$

FIG. 20. The ratio of the structure functions for neutrons for two ϵ values for π^+ and π^- at the $(W, Q^2, \epsilon_1, \epsilon_2)$ point (2.2, 1.2, 0.94, 0.96).
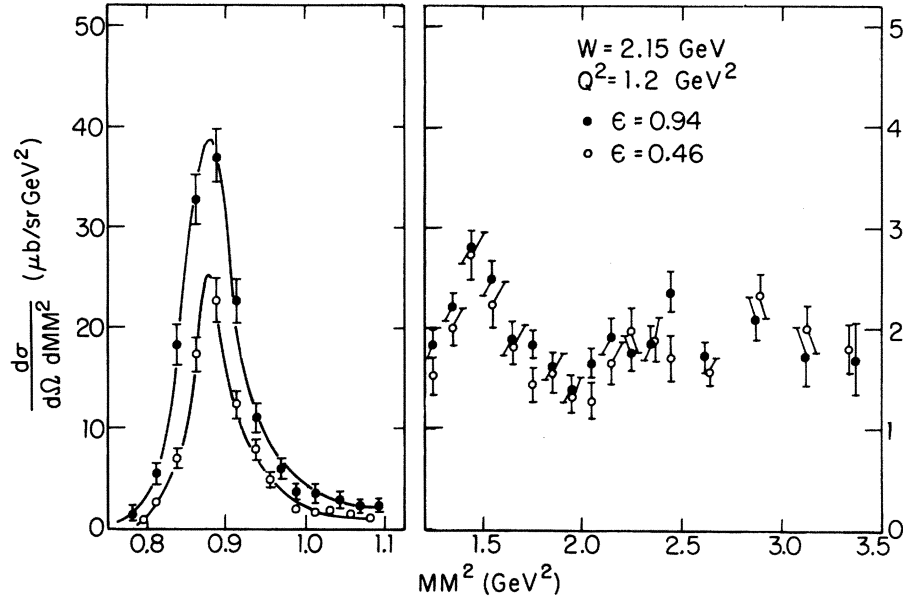
FIG. 21. Sample missing-mass-squared spectra with $|t - t_{min}| < 0.02$ GeV^2 for two values of ϵ where t is the momentum transfer squared from the photon to the pion. The high-ϵ results are from Ref. 18 and the low-ϵ results are from the present experiment.

This is most easily evaluated in terms of the rapidity

$$y = -\tfrac{1}{2}\ln\left(\frac{E^* + p_L^*}{E^* - p_L^*}\right).$$ (64)

Then

$$\langle n \rangle = \tfrac{1}{2}\int_{x'>0} \frac{E}{\sigma_{tot}} \frac{d^3\sigma}{dp^3} \, d\phi \, dp_T^2 dy$$

$$\simeq \frac{\pi}{b}\int_{x'>0} F(y)dy,$$ (65)

TABLE X. Ratio of high-ϵ to low-ϵ invariant cross sections.

W (GeV)	Q^2 (GeV^2)	ω	ϵ_1	ϵ_2	$(A + \epsilon_1 C)/(A + \epsilon_2 C)$				
					$0.0 < x' < 0.3$	$0.3 < x' < 0.5$	$0.5 < x' < 0.7$	$0.7 < x' < 0.9$	$0.3 < x' < 0.7$
					(a) π^+ from protons				
2.2	1.2	4.1	0.94	0.45	1.35 ± 0.22	0.93 ± 0.06	1.10 ± 0.06	1.11 ± 0.05	0.99 ± 0.05
2.7	2.0	4.2	0.81	0.34	1.12 ± 0.12	1.15 ± 0.07	0.97 ± 0.06	1.20 ± 0.07	1.08 ± 0.05
2.7	3.3	2.9	0.81	0.38	1.68 ± 0.42	1.09 ± 0.12	0.98 ± 0.10	1.01 ± 0.10	1.05 ± 0.08
					(b) π^- from protons				
2.2	1.2	4.1	0.94	0.45	1.39 ± 0.29	1.04 ± 0.09	1.07 ± 0.08	1.24 ± 0.08	1.05 ± 0.06
2.7	2.0	4.2	0.81	0.34	1.82 ± 0.60	0.98 ± 0.12	1.13 ± 0.14	1.33 ± 0.16	1.02 ± 0.09
2.7	3.3	2.9	0.81	0.38	$\cdots$	$\cdots$	0.91 ± 0.26	1.16 ± 0.28	0.91 ± 0.26
					(c) π^+ from deuterons				
2.2	1.2	4.1	0.94	0.45	0.93 ± 0.32	1.01 ± 0.07	1.13 ± 0.06	1.17 ± 0.05	1.06 ± 0.05
					(d) π^- from deuterons				
2.2	1.2	4.1	0.94	0.45	0.75 ± 0.18	0.96 ± 0.05	1.06 ± 0.05	1.31 ± 0.06	1.00 ± 0.04
					(e) π^+ from neutrons				
2.2	1.2	4.1	0.94	0.45	0.73 ± 0.53	1.16 ± 0.40	1.51 ± 0.27	1.42 ± 0.14	1.32 ± 0.26
					(f) π^- from neutrons				
2.2	1.2	4.1	0.94	0.45	0.64 ± 0.14	0.92 ± 0.12	1.09 ± 0.14	1.48 ± 0.23	0.97 ± 0.09

TABLE XI. Ratio of scalar to transverse cross sections.

W (GeV)	Q² (GeV²)	ω	ε₁	ε₂	C/A 0.0<x'<0.3	0.3<x'<0.5	0.5<x'<0.7	0.7<x'<0.9	0.3<x'<0.7
					(a) π⁺ from protons				
2.2	1.2	4.1	0.94	0.45	$1.10^{+1.51}_{-0.79}$	$-0.13^{+0.12}_{-0.10}$	$0.23^{+0.16}_{-0.14}$	$0.26^{+0.14}_{-0.12}$	$-0.02^{+0.10}_{-0.09}$
2.7	2.0	4.2	0.81	0.34	$0.28^{+0.34}_{-0.28}$	$0.35^{+0.18}_{-0.16}$	$-0.06^{+0.12}_{-0.11}$	$0.48^{+0.22}_{-0.20}$	$0.19^{+0.11}_{-0.11}$
2.7	3.3	2.9	0.81	0.38	$3.99^{+71.81}_{-3.18}$	$0.23^{+0.34}_{-0.28}$	$-0.05^{+0.22}_{-0.18}$	$0.03^{+0.25}_{-0.21}$	$0.12^{+0.22}_{-0.19}$
					(b) π⁻ from protons				
2.2	1.2	4.1	0.94	0.45	$1.40^{+3.39}_{-1.17}$	$0.09^{+0.22}_{-0.18}$	$0.16^{+0.21}_{-0.18}$	$0.64^{+0.31}_{-0.26}$	$0.12^{+0.16}_{-0.14}$
2.7	2.0	4.1	0.81	0.34	$\cdots$	$-0.05^{+0.26}_{-0.22}$	$0.30^{+0.41}_{-0.33}$	$0.91^{+0.70}_{-0.51}$	$0.04^{+0.22}_{-0.19}$
2.7	3.3	2.9	0.81	0.38	$\cdots$	$\cdots$	$-0.20^{+0.65}_{-0.42}$	$0.45^{+1.28}_{-0.69}$	$-0.20^{+0.65}_{-0.42}$
					(c) π⁺ from deuterium				
2.2	1.2	4.1	0.94	0.45	$-0.14^{+0.87}_{-0.47}$	$0.03^{+0.15}_{-0.13}$	$0.30^{+0.17}_{-0.15}$	$0.40^{+0.16}_{-0.14}$	$0.13^{+0.12}_{-0.11}$
					(d) π⁻ from deuterium				
2.2	1.2	4.1	0.94	0.45	$-0.43^{+0.28}_{-0.22}$	$-0.08^{+0.11}_{-0.10}$	$0.14^{+0.13}_{-0.12}$	$0.88^{+0.25}_{-0.21}$	$-0.01^{+0.08}_{-0.08}$
					(e) π⁺ from neutrons				
2.2	1.2	4.1	0.94	0.45	$-0.46^{+1.21}_{-0.51}$	$0.39^{+1.98}_{-0.79}$	$1.94^{+3.79}_{-1.34}$	$1.43^{+1.02}_{-0.65}$	$0.94^{+1.64}_{-0.80}$
					(f) π⁻ from neutrons				
2.2	1.2	4.1	0.94	0.45	$-0.58^{+0.19}_{-0.15}$	$-0.16^{+0.23}_{-0.19}$	$0.20^{+0.39}_{-0.30}$	$1.77^{+2.61}_{-1.13}$	$-0.06^{+0.19}_{-0.16}$

TABLE XII. Forward charged–hadron multiplicities.

W (GeV)	Q² (GeV²)	1/ω	$\langle n_{\pi^+} \rangle$	$\langle n_{\pi^-} \rangle$	$\langle n_p \rangle$	$\langle n \rangle$	$\langle n_c \rangle$	$\langle n_I \rangle$
			(a) Protons					
2.2	1.2	0.24	1.05±0.09	0.78±0.07	0.31±0.01	2.14±0.11	0.58±0.11	0.42±0.11
2.2[a]	1.2	0.24	0.87±0.05	0.61±0.09	0.20±0.01	1.68±0.10	0.46±0.10	0.36±0.10
2.2[a]	2.0	0.35	1.09±0.10	0.71±0.12	0.22±0.01	2.02±0.16	0.60±0.16	0.49±0.16
2.2[a]	4.0	0.53	0.93±0.09	0.57±0.08	0.21±0.01	1.71±0.12	0.57±0.12	0.46±0.12
2.7	2.0	0.24	1.08±0.06	0.67±0.04	0.22±0.01	1.96±0.07	0.63±0.07	0.52±0.07
2.7	3.3	0.35	1.12±0.04	0.66±0.03	0.22±0.01	2.00±0.06	0.67±0.06	0.56±0.06
2.7[a]	3.3	0.35	0.89±0.10	0.64±0.12	0.18±0.02	1.71±0.16	0.43±0.16	0.34±0.16
2.7	6.2	0.48	1.10±0.09	0.74±0.05	0.20±0.02	2.04±0.10	0.56±0.10	0.46±0.10
2.7	9.6	0.59	1.14±0.08	0.57±0.10	0.19±0.04	1.89±0.13	0.76±0.13	0.67±0.13
3.1[a]	1.2	0.12	1.13±0.08	0.80±0.06	0.10±0.01	2.03±0.10	0.42±0.10	0.38±0.10
3.1[a]	1.7	0.16	1.12±0.08	0.92±0.08	0.11±0.01	2.15±0.11	0.31±0.11	0.25±0.11
			(b) Neutrons					
2.2	1.2	0.24	0.75±0.18	1.21±0.13	0.21±0.03	2.17±0.22	−0.26±0.22	−0.36±0.22
2.2[a]	1.2	0.24	0.57±0.07	0.61±0.05	0.16±0.01	1.34±0.09	0.12±0.09	0.04±0.09
2.2[a]	4.0	0.53	0.68±0.14	0.73±0.13	0.15±0.03	1.56±0.19	0.10±0.19	0.02±0.19
2.7	2.0	0.24	1.01±0.14	1.18±0.09	0.18±0.02	2.37±0.17	0.02±0.17	−0.07±0.17
2.7	3.3	0.48	0.68±0.21	0.66±0.15	0.20±0.13	1.53±0.29	0.22±0.29	0.12±0.27
2.7	9.6	0.59	1.15±0.43	0.96±0.21	0.27±0.17	2.37±0.51	0.46±0.51	0.33±0.49
3.1[a]	1.2	0.12	0.56±0.06	0.62±0.06	0.09±0.01	1.27±0.09	0.03±0.09	−0.01±0.09

[a]References 19 and 24.

where F is the structure function for $p_T^2 \sim 0$ as a function of rapidity. The p_T^2-dependence parameter b comes from Eq. (51). In Table XII are shown the forward multiplicities for pions and protons[24] with $b_\pi = 6.0$ GeV^{-2} and $b_p = 3.4$ GeV^{-2} (see Ref. 58). The contribution due to kaons has not been included. Only K^+ were observed. The value of b_π used is consistent with the $\langle p_T^2 \rangle$ observed for small x', ~ 0.15 GeV^2 (see Ref. 26), which is the region which dominates the multiplicity. Experiments indicate that a smaller value of b_π should be used for $x' \gtrsim 0.3$ (see Ref. 26). Also shown in the table is the total forward charged-particle multiplicity. No W or Q^2 dependence is discernable. We also show the charge-weighted multiplicity $\langle n_c \rangle$ and the isospin-weighted multiplicity $\langle n_I \rangle$. In a simple quark model where the proton is dominated by the u quarks we expect $\langle n_c \rangle = \frac{2}{3}$ and $\langle n_I \rangle = \frac{1}{2}$. For a neutron we expect $\langle n_c \rangle = -\frac{1}{3}$ and $\langle n_I \rangle = -\frac{1}{2}$. In any quark model, these values are predicted for $x_B = 1/\omega = 1$.

Using the quark distribution functions from Eq. (23) we have calculated $\langle n_c \rangle$ and $\langle n_I \rangle$. It is assumed that the interacting quark's total charge and isospin appear in the forward hemisphere, $x > 0$. Then the data and theory will be directly comparable. To calculate the charge-weighted multiplicity from a proton target each quark's probability of interacting is weighted by its charge

$$\langle n_c \rangle_p = \frac{1}{f_{ep}(x_B)} \left(\frac{2}{3} \left\{ \frac{4}{9} [u(x_B) - \bar{u}(x_B)] \right\} - \frac{1}{3} \left\{ \frac{1}{9} [d(x_B) - \bar{d}(x_B)] \right\} \right.$$
$$\left. - \frac{1}{3} \left\{ \frac{1}{9} [s(x_B) - \bar{s}(x_B)] \right\} \right)$$

$$= \frac{1}{f_{ep}(x_B)} \left\{ \frac{2}{3} \left[\frac{4}{9} u_v(x_B) \right] - \frac{1}{3} \left[\frac{1}{9} d_v(x_B) \right] \right\}. \tag{66a}$$

Likewise, for the neutron charge multiplicity and the two isospin multiplicities we find

$$\langle n_c \rangle_n = \frac{1}{f_{en}(x_B)} \left\{ -\frac{1}{3} \left[\frac{1}{9} u_v(x_B) \right] + \frac{2}{3} \left[\frac{4}{9} d_v(x_B) \right] \right\}, \tag{66b}$$

$$\langle n_I \rangle_p = \frac{1}{f_{en}(x_B)} \left\{ \frac{1}{2} \left[\frac{4}{9} u_v(x_B) \right] - \frac{1}{2} \left[\frac{1}{9} d_v(x_B) \right] \right\}, \tag{66c}$$

$$\langle n_I \rangle_n = \frac{1}{f_{en}(x_B)} -\frac{1}{2} \left[\frac{1}{9} u_v(x_B) \right] + \frac{1}{2} \left[\frac{4}{9} d_v(x_B) \right] \right\}. \tag{66d}$$

We have evaluated Eqs. (66) and the results are shown in Fig. 22 with the data from this experiment and the earlier Harvard experiment. The agreement with the theory is reasonable but then the theory does not predict a dramatic effect in the data. Electroproduction experiments can obtain interesting information about the nucleon constituents from particle production in the forward
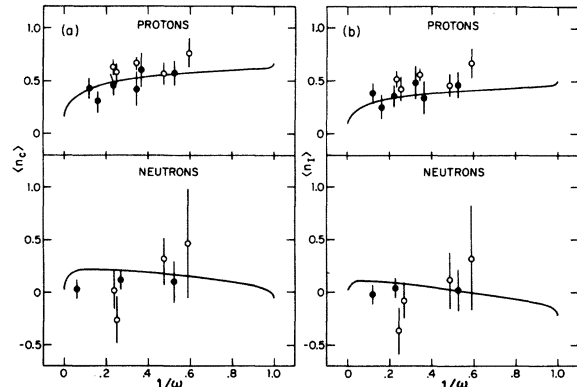

FIG. 22. (a) The charged-weighted forward multiplicity as a function of $1/\omega$ for proton and neutron targets. (b) The isospin-weighted forward multiplicity as a function of $1/\omega$ for proton and neutron targets. The open points are from the present experiment and the solid points are derived from Ref. 19. The curves are predictions of a quark model.

hemisphere. Ideally, such experiments would observe events over a large p_T range so that ad hoc assumptions about the p_T dependence do not have to be made.

VII. SUMMARY

(1) The π^+ structure function exhibits Feynman scaling and is independent of Q^2 at fixed ω; the π^- structure function shows a steepening x' dependence with increasing Q^2 and appears to exhibit Bjorken scaling for $W \gtrsim 2.5$ GeV.

(2) The production of π^+ from protons is greater than from neutrons while the reverse is true for π^- production.

(3) The charged-pion ratios scale in ω as predicted by quark-parton models. Scaling in W is not favored.

(4) The ratio of inclusive pion production by scalar photons to that by transverse photons is small and consistent with zero.

(5) The quark fragmentation functions are functions of x only, as assumed in certain quark models.

*Research supported in part by the U. S. Energy Research and Development Administration (Harvard) and in part by the National Science Foundation (Cornell).

†Present address: Fermi National Accelerator Laboratory, P. O. Box 500, Batavia, Illinois 60510.

‡Present address: 36 Webb Street, Lexington, Massachusetts 90029.

§Present address: Clinton P. Anderson Laboratory, Los Alamos, New Mexico 87544.

[1] R. Hofstadter, Rev. Mod. Phys. **28**, 214 (1956).

[2] G. Weber and R. E. Taylor, in *Proceedings of the Third International Symposium on Electron and Photon Interactions at High Energies, Stanford Linear Accelerator Center, Stanford, California, 1967*, edited by S. N. Berman (Clearing House of Federal Scientific and Technical Information, Washington, D. C., 1968); Richard Wilson, in *Proceedings of the 1971 International Symposium on Electron and Photon Interactions at High Energies*, edited by N. B. Mistry (Laboratory of Nuclear Studies, Cornell University, Ithaca, N. Y., 1972).

[3] E. D. Bloom, D. H. Coward, H. DeStaebler, J. Drees, G. Miller, L. W. Mo, R. E. Taylor, M. Breidenbach, J. I. Friedman, G. C. Hartmann, and H. W. Kendall, Phys. Rev. Lett. **23**, 930 (1969).

[4] J. I. Friedman and H. W. Kendall, Ann. Rev. Nucl. Sci. **22**, 203 (1972).

[5] G. Miller, E. D. Bloom, G. Buschhorn, D. H. Coward, H. DeStaebler, J. Drees, C. L. Jordan, L. W. Mo, R. E. Taylor, J. I. Friedman, G. C. Hartmann, H. W. Kendall, and R. Verdier, Phys. Rev. D **5**, 528 (1972).

[6] A. Bodek, M. Breidenbach, D. L. Dubin, J. E. Elias, J. I. Friedman, H. W. Kendall, J. S. Poucher, E. M. Riordan, M. R. Sogard, and D. H. Coward, Phys. Rev. Lett. **30**, 1087 (1973).

[7] J. D. Bjorken and E. A. Paschos, Phys. Rev. **185**, 1975 (1969).

[8] R. P. Feynman, *Photon-Hadron Interactions* (Benjamin, Reading, Mass., 1972).

[9] J. D. Bjorken, Phys. Rev. **179**, 1547 (1969).

[10] C. J. Bebek, A. Browman, C. N. Brown, K. M. Hanson, R. V. Kline, D. Larson, F. M. Pipkin, S. W. Raither, A. Silverman, and L. K. Sisterson, Phys. Rev. Lett. **37**, 1525 (1976).

[11] C. J. Bebek, A. Browman, C. N. Brown, K. M. Hanson, S. D. Holmes, R. V. Kline, D. Larson, F. M. Pipkin, S. W. Raither, A. Silverman, and L. K. Sisterson, Phys. Rev. Lett. **37**, 1320 (1976).

[12] C. J. Bebek, A. Browman, C. N. Brown, K. M. Hanson, R. V. Kline, D. Larson, F. M. Pipkin, S. W. Raither, A. Silverman, and L. K. Sisterson, Phys. Rev. Lett. **38**, 1051 (1977).

[13] L. S. Rochester, W. B. Atwood, E. D. Bloom, R. L. A. Cottrell, D. H. Coward, H. DeStaebler, M. Mestayer, C. Y. Prescott, S. Stein, R. E. Taylor, and D. Trines, Phys. Rev. Lett. **36**, 1284 (1976); D. L. Fancher, D. L. Caldwell, J. P. Cumalat, A. M. Eisner, T. P. McPharlin, R. J. Morrison, F. V. Murphy, and S. J. Yellin, *ibid.* **37**, 1323 (1976).

[14] L. N. Hand, Phys. Rev. **129**, 1834 (1963).

[15] S. M. Berman, Phys. Rev. **135**, 1249 (1964).

[16] N. Dombey, Rev. Mod. Phys. **41**, 236 (1969).

[17] R. P. Feynman, Phys. Rev. Lett. **23**, 1415 (1969).

[18] C. J. Bebek, C. N. Brown, C. A. Lichtenstein, M. Herzlinger, F. M. Pipkin, L. K. Sisterson,

D. Andrews, K. Berkelman, D. G. Cassel, and D. L. Hartill, Phys. Rev. Lett. **30**, 624 (1973); and Nucl. Phys. **B75**, 20 (1974).

[19] C. J. Bebek, C. N. Brown, M. Herzlinger, S. D. Holmes, C. A. Lichtenstein, F. M. Pipkin, S. W. Raither, and L. K. Sisterson, Phys. Rev. Lett. **34**, 759 (1975); and Phys. Rev. D **15**, 3085 (1977).

[20] R. McElhaney and S. F. Tuan, Phys. Rev. D **8**, 2267 (1973).

[21] J. Cleymans and R. Rodenberg, Phys. Rev. D **9**, 155 (1974).

[22] J. Benecke, T. T. Chou, C. N. Yang, and E. Yen, Phys. Rev. **188**, 2159 (1969).

[23] C. J. Bebek, C. N. Brown, M. Herzlinger, C. A. Lichtenstein, F. M. Pipkin, L. K. Sisterson, D. Andrews, K. Berkelman, D. G. Cassel, and D. L. Hartill, Phys. Rev. Lett. **32**, 27 (1974).

[24] C. J. Bebek, C. N. Brown, M. Herzlinger, S. D. Holmes, C. A. Lichtenstein, F. M. Pipkin, S. Raither, and L. K. Sisterson, Phys. Rev. Lett. **34**, 1115 (1975).

[25] H. Ackermann, T. Azemoon, W. Gabriel, D. Lüke, G. Specht, E. Ganssauge, F. Janata, H. D. Mertiens, H. D. Reich, and D. Schmidt, DESY Report No. 76/44, 1976 (unpublished).

[26] G. Wolf, in *Proceedings of the 1975 International Symposium on Lepton and Photon Interactions at High Energies, Stanford, California*, edited by W. T. Kirk (SLAC, Stanford, 1975), p. 795.

[27] S. D. Drell, D. J. Levy, and T.-M. Yan, Phys. Rev. **187**, 2159 (1969).

[28] F. Gutbrod and U. E. Schröder, Nucl. Phys. **B62**, 381 (1973).

[29] V. I. Zakarov, in *Proceedings of the XVIII International Conference on High Energy Physics, Tbilisi, 1976*, edited by N. N. Bogolubov *et al.* (JINR, Dubna, U.S.S.R., 1976).

[30] F. Ravndal, Phys. Lett. **43B**, 301 (1973).

[31] J. T. Dakin, G. J. Feldman, F. Martin, M. L. Perl, and W. T. Toner, Phys. Rev. D **10**, 1401 (1974).

[32] H. L. Anderson, V. K. Bharadwaj, N. E. Booth, R. M. Fine, W. R. Francis, B. A. Gordon, R. H. Heisterberg, R. G. Hicks, T. B. W. Kirk, G. I. Kirkbride, W. A. Loomis, H. S. Matis, L. W. Mo, L. C. Myrianthopoulos, F. M. Pipkin, S. H. Pordes, T. W. Quirk, W. D. Shambroom, A. Skuja, L. J. Verhey, W. S. C. Wright, Richard Wilson, and S. C. Wright, Phys. Rev. Lett. **36**, 1422 (1976).

[33] J. T. Dakin and G. J. Feldman, Phys. Rev. D **8**, 2862 (1973).

[34] R. Hagedorn, Nucl. Phys. **B24**, 93 (1970).

[35] F. Brasse, in *Proceedings of the Sixth International Symposium on Electron and Photon Interactions at High Energies, Bonn, Germany, 1973*, edited by H. Rollink and W. Pfeil (North-Holland, Amsterdam, 1974).

[36] C. G. Callan and D. J. Gross, Phys. Rev. Lett. **22**, 156 (1969).

[37] E. M. Riordan, A. Bodek, M. Breidenbach, D. L. Dubin, J. E. Elias, J. I. Friedman, H. W. Kendall, J. S. Poucher, M. R. Sogard, and D. H. Coward, Phys. Rev. Lett. **33**, 561 (1974).

[38] O. Nachtmann, Phys. Rev. D **5**, 686 (1972).

[39] E. D. Bloom, in *Proceedings of the Sixth International Symposium on Electron and Photon Interactions at High Energies, Bonn, Germany, 1973* (Ref. 35).

[40]J. J. Sakurai, Phys. Rev. Lett. 22, 981 (1969).

[41]C. J. Bebek, A. Browman, C. N. Brown, K. M. Hanson, R. V. Kline, D. Larson, F. M. Pipkin, S. W. Raither, A. Silverman, and L. K. Sisterson, Phys. Rev. D 15, 3077 (1977).

[42]H. Harari, in *Proceedings of the 1971 International Symposium on Electron and Photon Interactions at High Energies* (Ref. 2).

[43]W. B. Atwood, private communication. Defining $x = (2M\nu + 1.267)/(Q^2 + 0.3589)$ and $y = (1 - 1/x)$ the fit is $\nu W_2 = (x/\omega)y^3 (1.04 - 1.667y + 8.966y^2 - 14.46y^3 + 6.557y^4)$. This is valid for $W \gtrsim 2$ GeV.

[44]L. Hulthén and M. Sugawara, *Handbuch der Physik*, edited by S. Flügge (Springer, Berlin, 1957), Vol. XXXIX.

[45]R. J. Glauber, Phys. Rev. 100, 242 (1955); V. Franco and R. J. Glauber, *ibid.* 142, 1195 (1966).

[46]L. W. Mo and Y. S. Tsai, Rev. Mod. Phys. 41, 205 (1969).

[47]W. A. Loomis, H. S. Matis, H. L. Anderson, V. K. Bharadwaj, N. E. Booth, F. M. Fine, W. R. Francis, B. A. Gordon, R. H. Heisterberg, R. G. Hicks, T. B. W. Kirk, G. I. Kirkbride, L. W. Mo, L. C. Myrianthopoulos, F. M. Pipkin, S. H. Pordes, T. W. Quirk, W. D. Shambroom, A. Skuja, L. J. Verhey, and W. S. C. Williams, Phys. Rev. Lett. 35, 1483 (1975).

[48]P. Bosetti, H. Grässler, H. Kirk, M. Matziolis, U. Gensch, P. Kostka, K. Böckmann, G. J. Bossen, J. Lowsky, M. Rost, T. Besliu, V. T. Cocconi, P. F. Dalpiaz, P. Duinker, S. Matsumoto, D. R. O. Morrison, R. Stroynowski, H. Wahl, T. Coghen, W. Zielinski, S. Brandt, M. Bardadin-Otwinowska, and T. Hofmokl, Nucl. Phys. B54, 141 (1973).

[49]A. Browman, K. M. Hanson, St D. Holmes, R. V. Kline, D. Larson, F. M. Pipkin, S. W. Raither, and A. Silverman, Phys. Rev. Lett. 37, 651 (1976).

[50]J. Gandsman, G. Alexander, S. Dagan, L. D. Jacobs, A. Levy, D. Lissauer, and L. M. Rosenstein, Nucl.

Phys. B61, 32 (1973).

[51]H. L. Anderson, V. K. Bharadwaj, N. E. Booth, R. M. Fine, W. R. Francis, B. A. Gordon, R. H. Heisterberg, R. G. Hicks, T. B. W. Kirk, G. I. Kirkbride, W. A. Loomis, H. S. Matis, L. W. Mo, L. C. Myrianthopoulos, F. M. Pipkin, S. H. Pordes, T. W. Quirk, W. D. Shambroom, A. Skuja, L. J. Verhey, W. S. C. Williams, Richard Wilson, and S. C. Wright, unpublished work.

[52]I. Dammann, C. Driver, K. Heinloth, G. Hofmann, F. Janata, P. Karow, D. Lüke, D. Schmidt, and G. Specht, Nucl. Phys. B54, 381 (1973).

[53]J. C. Adler, F. W. Brasse, E. Chazelas, W. Fehrenbach, W. Flauger, K. H. Frank, E. Ganssauge, J. Gayler, V. Korbel, W. Krechlok, J. May, M. Merkwitz, and P. D. Zimmerman, Nucl. Phys. B46, 415 (1972).

[54]J. F. Martin, C. Bolon, R. C. Lanza, D. Luckey, L. S. Osborne, D. G. Roth, G. J. Feldman, G. Hanson, D. E. Lyon, M. L. Perl, T. Pun, and J. T. Dakin, Phys. Lett. 65B, 483 (1976).

[55]J. P. Berge, D. Bogert, D. C. Cundy, F. A. DiBianca, A. Dunaitsev, V. Efremenko, P. Ermolov, W. Fowler, R. Hanft, G. Harigel, F. R. Huson, V. Kolganov, A. Mukhin, F. A. Nezrick, Y. Rjabov, W. G. Scott, W. Smart, C. T. Coffin, R. N. Diamond, H. French, W. Louis, B. P. Roe, A. A. Seidl, and J. C. Vander Velde, Fermilab Report No. FERMILAB-PUB-75/84-EXP (7300.045) (unpublished).

[56]C. J. Bebek, C. N. Brown, M. Herzlinger, S. D. Holmes, C. A. Lichtenstein, F. M. Pipkin, S. Raither, and L. K. Sisterson, Phys. Rev. D 13, 25 (1976).

[57]R. E. Taylor, in *Proceedings of the 1975 International Symposium on Lepton and Photon Interactions at High Energies, Stanford, California* (Ref. 26).

[58]H. Burfeindt, G. Buschhorn, H. Genzel, P. Heide, U. Kötz, K.-H. Mess, P. Schmüser, B. Sonne, G. Vogel, and B. H. Wiik, Nucl. Phys. B74, 189 (1974).